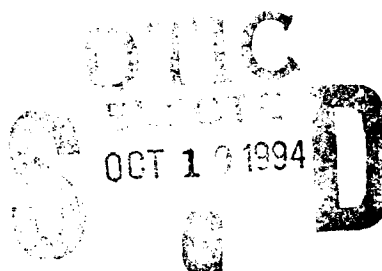




A Model of an Infinite Length, Axisymmetric, Isotropic, Forced Thick Shell

Andrew J. Hull
Submarine Sonar Department

AD-A285 586



3919 94-32492



Naval Undersea Warfare Center Division
Newport, Rhode Island

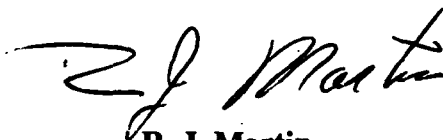
PREFACE

This investigation described in this report was sponsored by the Office of Naval Research.

The technical reviewer for this report was S. A. Austin (Code 2141).

The author wishes to thank Karen Holt (Code 0251), NUWC Detachment New London, for her help with the technical editing.

REVIEWED AND APPROVED: 22 August 1994

A handwritten signature in black ink, appearing to read 'R. J. Martin', is positioned above the printed name.

R. J. Martin
Acting Head, Submarine Sonar Department

REPORT DOCUMENTATION PAGEForm Approved
OMB No. 0704-0188

Public reporting burden for this collection of information is estimated to average 1 hour per response, including the time for reviewing instructions, searching existing data sources, gathering and maintaining the data needed, and completing and reviewing the collection of information. Send comments regarding this burden estimate or any other aspect of this collection of information, including suggestions for reducing this burden, to Washington Headquarters Services, Directorate for Information Operations and Reports, 1215 Jefferson Davis Highway, Suite 1204, Arlington, VA 22202-4302, and to the Office of Management and Budget, Paperwork Reduction Project (0704-0188), Washington, DC 20503.

1. AGENCY USE ONLY (Leave Blank)		2. REPORT DATE 22 August 1994	3. REPORT TYPE AND DATES COVERED Final	
4. TITLE AND SUBTITLE A Model of an Infinite Length, Axisymmetric, Isotropic, Forced Thick Shell			5. FUNDING NUMBERS	
6. AUTHOR(S) Andrew J. Hull				
7. PERFORMING ORGANIZATION NAME(S) AND ADDRESS(ES) Naval Undersea Warfare Center Detachment New London New London, Connecticut 06320			8. PERFORMING ORGANIZATION REPORT NUMBER TR 10,719	
9. SPONSORING/MONITORING AGENCY NAME(S) AND ADDRESS(ES) Office of Naval Research 800 North Quincy St. Arlington, VA 22217			10. SPONSORING/MONITORING AGENCY REPORT NUMBER	
11. SUPPLEMENTARY NOTES				
12a. DISTRIBUTION/AVAILABILITY STATEMENT Approved for public release; distribution is unlimited.			12b. DISTRIBUTION CODE	
13. ABSTRACT (Maximum 200 words) The model described in this report provides an exact solution to the equations of motion for an infinite length, axisymmetric, isotropic, forced thick shell. In this model, the governing equations of motion of an isotropic elastic solid in cylindrical coordinates are first separated into a dilatational wave equation and three distortional wave equations that can be solved with Bessel functions. These general solutions are then inserted into stress-strain constitutive equations at the interior and exterior of the shell. The displacements are next determined from forcing functions that are applied to the shell. In this new model, the shell thickness effects on wave propagation are addressed. The case where the mean radius of the shell is equal to its thickness has been analyzed and compared with thin shell equations of motion. It is shown that, in general, the thin shell equations of motion often underpredict thick shell response.				
14. SUBJECT TERMS Axisymmetric Shell, Elastic Solid, Equations of Motion, Forced Thick Shell, Infinite Length Shell, Isotropic Solid, Stress-Strain Equations, Thick Shell, Thin Shell, Wave Equation			15. NUMBER OF PAGES 44	
			16. PRICE CODE	
17. SECURITY CLASSIFICATION OF REPORT UNCLASSIFIED	18. SECURITY CLASSIFICATION OF THIS PAGE UNCLASSIFIED	19. SECURITY CLASSIFICATION OF ABSTRACT UNCLASSIFIED	20. LIMITATION OF ABSTRACT SAR	

TABLE OF CONTENTS

	Page
LIST OF ILLUSTRATIONS.....	ii
1 INTRODUCTION.....	1
2 SYSTEM MODEL.....	2
3 MODEL VALIDATION.....	15
4 ANALYSIS.....	20
5 CONCLUSIONS.....	30
6 REFERENCES.....	30
APPENDIX - DERIVATIVES OF THE BESSEL FUNCTIONS.....	A-1

Accession For	
NTIS CRA&I	<input checked="" type="checkbox"/>
DTIC TAB	<input type="checkbox"/>
Unannounced	<input type="checkbox"/>
Justification	
By	
Distribution /	
Availability Codes	
Dist	Avail and/or Special
A-1	

LIST OF ILLUSTRATIONS

Figure		Page
1	Cylindrical Shell.....	3
2	Relationship of Bessel Function Regions to Wave Speeds.....	7
3	Magnitude of Axial Displacement Divided by Applied Axial Stress: Comparison of Thick Shell Model to Thin Shell Model, $f = 50$ Hz, $h/a = 1/100$	18
4	Magnitude of Radial Displacement Divided by Applied Axial Stress: Comparison of Thick Shell Model to Thin Shell Model, $f = 50$ Hz, $h/a = 1/100$	18
5	Magnitude of Axial Displacement Divided by Applied Radial Pressure: Comparison of Thick Shell Model to Thin Shell Model, $f = 50$ Hz, $h/a = 1/100$	19
6	Magnitude of Radial Displacement Divided by Applied Radial Pressure: Comparison of Thick Shell Model to Thin Shell Model, $f = 50$ Hz, $h/a = 1/100$	19
7	Magnitude of Axial Displacement Divided by Applied Axial Stress: Comparison of Thick Shell Model to Thin Shell Model, $f = 50$ Hz, $2h/(a+b) = 1$...	22
8	Magnitude of Radial Displacement Divided by Applied Axial Stress: Comparison of Thick Shell Model to Thin Shell Model, $f = 50$ Hz, $2h/(a+b) = 1$...	22
9	Magnitude of Axial Displacement Divided by Applied Radial Pressure: Comparison of Thick Shell Model to Thin Shell Model, $f = 50$ Hz, $2h/(a+b) = 1$...	23
10	Magnitude of Radial Displacement Divided by Applied Radial Pressure: Comparison of Thick Shell Model to Thin Shell Model, $f = 50$ Hz, $2h/(a+b) = 1$...	23
11	Magnitude of Axial Displacement Divided by Applied Axial Stress: Comparison of Thick Shell Model to Thin Shell Model, $f = 500$ Hz, $2h/(a+b) = 1$..	24
12	Magnitude of Radial Displacement Divided by Applied Axial Stress: Comparison of Thick Shell Model to Thin Shell Model, $f = 500$ Hz, $2h/(a+b) = 1$..	24
13	Magnitude of Axial Displacement Divided by Applied Radial Pressure: Comparison of Thick Shell Model to Thin Shell Model, $f = 500$ Hz, $2h/(a+b) = 1$..	25
14	Magnitude of Radial Displacement Divided by Applied Radial Pressure: Comparison of Thick Shell Model to Thin Shell Model, $f = 500$ Hz, $2h/(a+b) = 1$..	25
15	Magnitude of Axial Displacement Divided by Applied Axial Stress: Comparison of Transfer Function at $r = a$ to $r = b$, $f = 50$ Hz, $2h/(a+b) = 1$	26

LIST OF ILLUSTRATIONS (CONT'D)

Figure		Page
16	Magnitude of Radial Displacement Divided by Applied Axial Stress: Comparison of Transfer Function at $r = a$ to $r = b$, $f = 50$ Hz, $2h/(a+b) = 1$	26
17	Magnitude of Axial Displacement Divided by Applied Radial Pressure: Comparison of Transfer Function at $r = a$ to $r = b$, $f = 50$ Hz, $2h/(a+b) = 1$	27
18	Magnitude of Radial Displacement Divided by Applied Radial Pressure: Comparison of Transfer Function at $r = a$ to $r = b$, $f = 50$ Hz, $2h/(a+b) = 1$	27
19	Magnitude of Axial Displacement Divided by Applied Axial Stress: Comparison of Transfer Function at $r = a$ to $r = b$, $f = 500$ Hz, $2h/(a+b) = 1$	28
20	Magnitude of Radial Displacement Divided by Applied Axial Stress: Comparison of Transfer Function at $r = a$ to $r = b$, $f = 500$ Hz, $2h/(a+b) = 1$	28
21	Magnitude of Axial Displacement Divided by Applied Radial Pressure: Comparison of Transfer Function at $r = a$ to $r = b$, $f = 500$ Hz, $2h/(a+b) = 1$	29
22	Magnitude of Radial Displacement Divided by Applied Radial Pressure: Comparison of Transfer Function at $r = a$ to $r = b$, $f = 500$ Hz, $2h/(a+b) = 1$	29

A MODEL OF AN INFINITE LENGTH, AXISYMMETRIC, ISOTROPIC, FORCED THICK SHELL

1. INTRODUCTION

The displacement field and wave propagation of elastic shells have been studied by numerous researchers because of the use of such shells in many mechanical designs. A common solution is to model the shell as unforced and infinitely long in order to determine its free wave propagation characteristics (Herrmann and Mirsky, 1956; Mirsky, 1964a). Another technique approximates the shell equations of motion and derives a forced response (Mirsky, 1964b; McNiven et al., 1966). Although the free wave propagation approach is useful for unforced systems, it does not account for shell loading at the boundary. However, the forced wave method is based on approximations to the system that are not always accurate.

In this report, the analysis of an infinite length, axisymmetric, isotropic, forced thick shell is presented. The derivation begins with the partial differential equations of motion of an isotropic elastic solid in cylindrical coordinates. The shell displacements are written as a sum of a dilatational component and an equivoluminal vector component. This approach allows the equations to be separated into a dilatational wave equation and three distortional (shear) wave equations. General solutions to these four wave equations are then determined. These general solutions are inserted into the stress-strain relationships at the inner and outer diameter of the shell and equated to the externally applied loading function on the shell. Based on these relationships, a four-by-four system of linear equations is developed. The solution to the linear equations yields the displacements of the shell.

Corresponding to an extremely long cylinder with external forcing at a definite wavenumber and frequency, the model has been derived to address shell thickness effects on wave propagation. Two specific cases are investigated: the first is an extremely thin shell and the second is a shell where the mean radius is equal to the thickness.

2. SYSTEM MODEL

The system model is a cylindrical, linear, isotropic, elastic medium whose motion is governed by the equation (Timoshenko and Goodier, 1934)

$$\mu \nabla^2 \mathbf{u} + (\lambda + \mu) \nabla \nabla \cdot \mathbf{u} = \rho \frac{\partial^2 \mathbf{u}}{\partial t^2}, \quad (1)$$

where ρ is the density; λ and μ are the Lamé constants; t is time; \cdot denotes a vector dot product; \mathbf{u} is the cylindrical coordinate displacement vector expressed as

$$\mathbf{u} = \begin{Bmatrix} u_r(r, \theta, z, t) \\ u_\theta(r, \theta, z, t) \\ u_z(r, \theta, z, t) \end{Bmatrix}, \quad (2)$$

with subscript r denoting the radial direction, θ denoting the angular direction, and z denoting the axial direction; ∇ is the gradient vector differential operator written in cylindrical coordinates as (Potter, 1978)

$$\nabla = \frac{\partial}{\partial r} i_r + \frac{1}{r} \frac{\partial}{\partial \theta} i_\theta + \frac{\partial}{\partial z} i_z, \quad (3)$$

with i_r denoting the unit vector in the r direction, i_θ denoting the unit vector in the θ direction, and i_z denoting the unit vector in the z direction; ∇^2 is the three-dimensional Laplace operator operating on vector \mathbf{u} as

$$\nabla^2 \mathbf{u} = \left(\nabla^2 u_r - \frac{u_r}{r^2} - \frac{2}{r^2} \frac{\partial u_\theta}{\partial \theta} \right) i_r + \left(\nabla^2 u_\theta - \frac{u_\theta}{r^2} + \frac{2}{r^2} \frac{\partial u_r}{\partial \theta} \right) i_\theta + \nabla^2 u_z i_z, \quad (4)$$

with ∇^2 operating on scalar u as

$$\nabla^2 u_{r,\theta,z} = \nabla \cdot \nabla u_{r,\theta,z} = \frac{1}{r} \frac{\partial}{\partial r} \left(r \frac{\partial u_{r,\theta,z}}{\partial r} \right) + \frac{1}{r^2} \frac{\partial^2 u_{r,\theta,z}}{\partial \theta^2} + \frac{\partial^2 u_{r,\theta,z}}{\partial z^2}; \quad (5)$$

and the term $\nabla \cdot \mathbf{u}$ is called the divergence and is equal to

$$\nabla \cdot \mathbf{u} = \frac{\partial u_r}{\partial r} + \frac{1}{r} \frac{\partial u_\theta}{\partial \theta} + \frac{\partial u_z}{\partial z} + \frac{u_r}{r}. \quad (6)$$

The coordinate system of the shell is shown in figure 1.

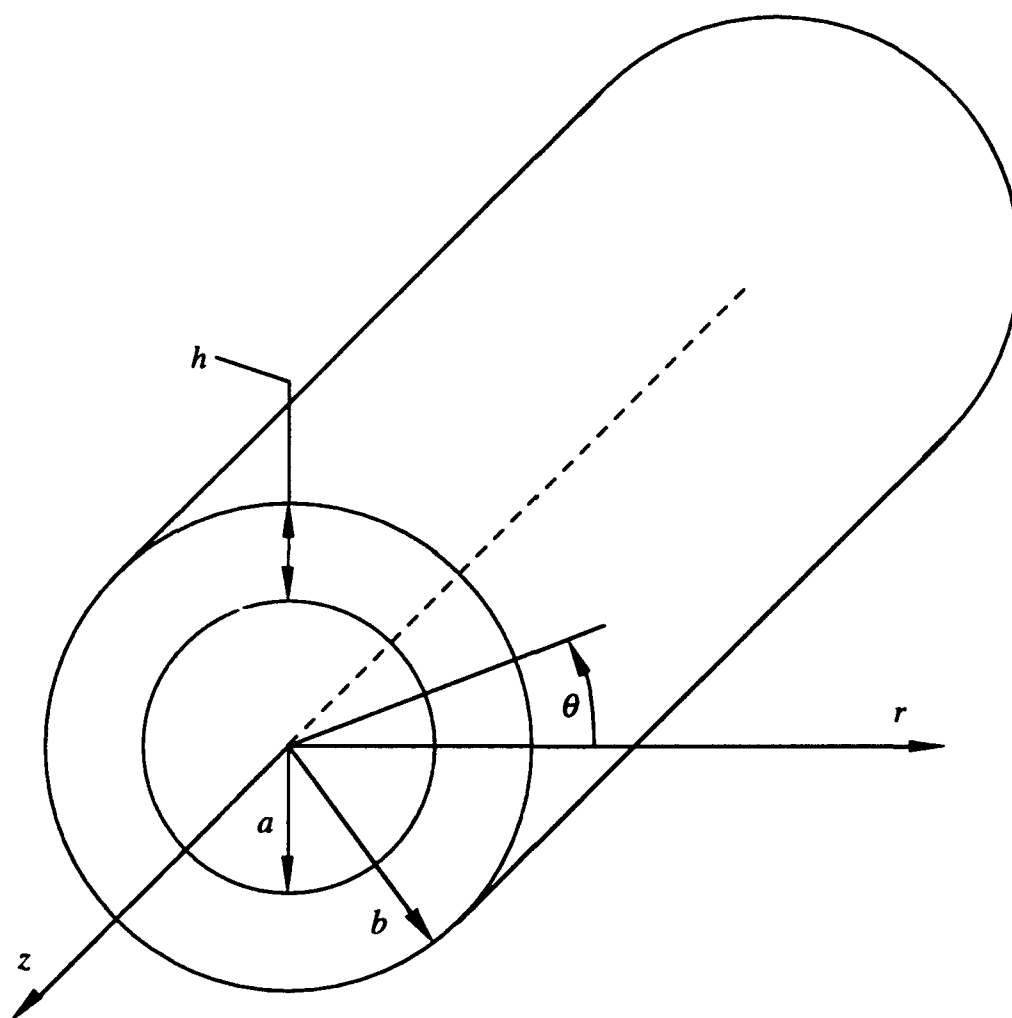


Figure 1. Cylindrical Shell

The displacement vector \mathbf{u} is written as

$$\mathbf{u} = \nabla \phi + \nabla \times \mathbf{H} , \quad (7)$$

where ϕ is a dilatational scalar potential, \times denotes a vector cross-product, and \mathbf{H} is an equivoluminal vector potential expressed as

$$\mathbf{H} = \begin{Bmatrix} H_r(r, \theta, z, t) \\ H_\theta(r, \theta, z, t) \\ H_z(r, \theta, z, t) \end{Bmatrix} . \quad (8)$$

Expanding equation (7) and breaking the displacement vector into its individual terms yields

$$u_r = \frac{\partial \phi}{\partial r} + \frac{1}{r} \frac{\partial H_z}{\partial \theta} - \frac{\partial H_\theta}{\partial z} , \quad (9)$$

$$u_\theta = \frac{1}{r} \frac{\partial \phi}{\partial \theta} + \frac{\partial H_r}{\partial z} - \frac{\partial H_z}{\partial r} , \quad (10)$$

and

$$u_z = \frac{\partial \phi}{\partial z} + \frac{H_\theta}{r} + \frac{\partial H_\theta}{\partial r} - \frac{1}{r} \frac{\partial H_r}{\partial \theta} . \quad (11)$$

Equation (7) is inserted into equation (1), which results in

$$c_d^2 \nabla^2 \phi = \frac{\partial^2 \phi}{\partial t^2} \quad (12)$$

and

$$c_s^2 \nabla^2 \mathbf{H} = \frac{\partial^2 \mathbf{H}}{\partial t^2} . \quad (13)$$

The constants c_d and c_s are the dilatational and shear wave speeds, respectively, and are determined by

$$c_d = \sqrt{\frac{\lambda + 2\mu}{\rho}} \quad (14)$$

and

$$c_s = \sqrt{\frac{\mu}{\rho}} . \quad (15)$$

The conditions of infinite length, axisymmetric response ($n = 0$), and steady-state response are now imposed, allowing the scalar and vector potential to be written as

$$\phi = g(r)\cos(n\theta)e^{ikz}e^{i\omega t} = g(r)e^{ikz}e^{i\omega t} , \quad (16)$$

$$H_r = h_r(r)\sin(n\theta)e^{ikz}e^{i\omega t} \equiv 0 , \quad (17)$$

$$H_\theta = h_\theta(r)\cos(n\theta)e^{ikz}e^{i\omega t} = h_\theta(r)e^{ikz}e^{i\omega t} , \quad (18)$$

and

$$H_z = h_z(r)\sin(n\theta)e^{ikz}e^{i\omega t} \equiv 0 , \quad (19)$$

where k is the wavenumber of excitation, ω is the frequency of excitation, and i is the square root of -1. Note that for axisymmetric response, the equations of motion are dependent only on the scalar potential ϕ and angular contribution H_θ of the vector potential. Additionally, because $H_r = 0$ and $H_z = 0$, and H_θ and ϕ are not functions of θ , equation (10) becomes

$$u_\theta = \frac{\partial(\)}{\partial\theta} = 0 , \quad (20)$$

where () denotes any function. Inserting equations (16)-(19) into equations (12) and (13) yields the following four wave equations:

$$\frac{d^2 g(r)}{dr^2} + \frac{1}{r} \frac{dg(r)}{dr} + \left(\frac{\omega^2}{c_d^2} - k^2 \right) g(r) = 0 , \quad (21)$$

$$\frac{d^2 h_r(r)}{dr^2} + \frac{1}{r} \frac{dh_r(r)}{dr} + \left(\frac{\omega^2}{c_s^2} - k^2 - \frac{1}{r^2} \right) h_r(r) = 0 , \quad (22)$$

$$\frac{d^2 h_\theta(r)}{dr^2} + \frac{1}{r} \frac{dh_\theta(r)}{dr} + \left(\frac{\omega^2}{c_s^2} - k^2 - \frac{1}{r^2} \right) h_\theta(r) = 0 , \quad (23)$$

and

$$\frac{d^2 h_z(r)}{dr^2} + \frac{1}{r} \frac{dh_z(r)}{dr} + \left(\frac{\omega^2}{c_s^2} - k^2 \right) h_z(r) = 0 . \quad (24)$$

Equations (21) and (23) are now solved with Bessel functions. No solution is found to equations (22) and (24) because they do not contribute to the axisymmetric response. The solution to equation (21) is

$$g(r) = \begin{cases} C_1 J_0(\alpha r) + C_2 Y_0(\alpha r), & |k| < \frac{\omega}{c_d}, \\ C_1 I_0(\alpha r) + C_2 K_0(\alpha r), & |k| > \frac{\omega}{c_d}, \end{cases} \quad (25)$$

where J_0 is a zero-order, first-kind standard Bessel function; Y_0 is a zero-order, second-kind standard Bessel function; I_0 is a zero-order, first-kind modified Bessel function; K_0 is a zero-order, second-kind modified Bessel function; C_1 and C_2 are constants (determined below); and

$$\alpha = \sqrt{\left| \frac{\omega^2}{c_d^2} - k^2 \right|}. \quad (26)$$

The solution to equation (23) is

$$h_\theta(r) = \begin{cases} C_3 J_1(\beta r) + C_4 Y_1(\beta r), & |k| < \frac{\omega}{c_s}, \\ C_3 I_1(\beta r) + C_4 K_1(\beta r), & |k| > \frac{\omega}{c_s}, \end{cases} \quad (27)$$

where J_1 is a first-order, first-kind standard Bessel function; Y_1 is a first-order, second-kind standard Bessel function; I_1 is a first-order, first-kind modified Bessel function; K_1 is a first-order, second-kind modified Bessel function; C_3 and C_4 are constants (determined below); and

$$\beta = \sqrt{\left| \frac{\omega^2}{c_s^2} - k^2 \right|}. \quad (28)$$

Based on the solutions shown in equations (25) and (27), three distinct wavenumber regions are dependent on the dilatational and shear wave speeds. In these low, medium, and high wavenumber regions, the solution set changes between standard and modified Bessel functions as shown in figure 2.

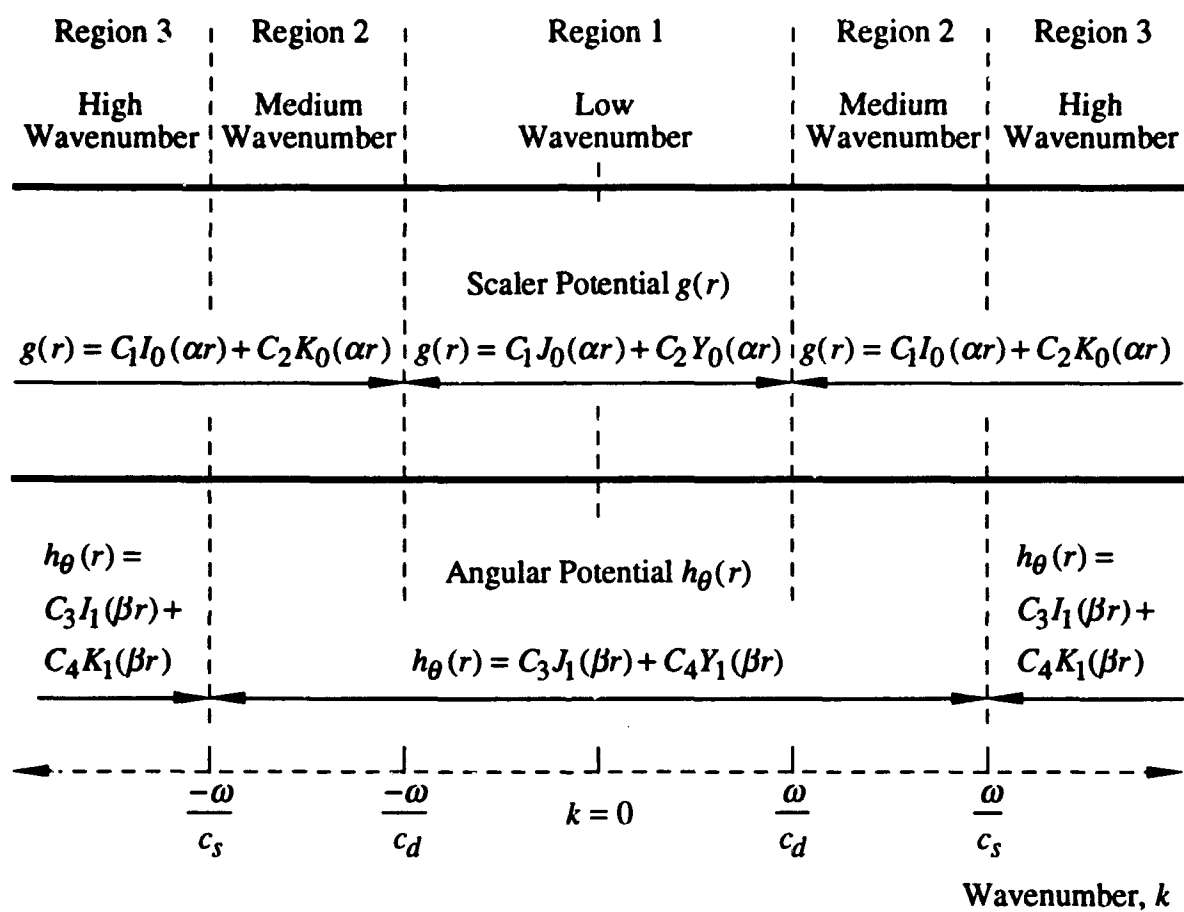


Figure 2. Relationship of Bessel Function Regions to Wave Speeds

The displacements and external forces are now equated by use of the stress-strain constitutive equations on the forced surfaces of the shell. The normal stress, strain, and radial forces acting on the cylinder are related by

$$\sigma_{rr}(a, \theta, z, t) - (\lambda + 2\mu)\epsilon_{rr}(a, \theta, z, t) + \lambda\epsilon_{\theta\theta}(a, \theta, z, t) + \lambda\epsilon_{zz}(a, \theta, z, t) = p(a, \theta, z, t) \quad (29)$$

and

$$\sigma_{rr}(b, \theta, z, t) - (\lambda + 2\mu)\epsilon_{rr}(b, \theta, z, t) + \lambda\epsilon_{\theta\theta}(b, \theta, z, t) + \lambda\epsilon_{zz}(b, \theta, z, t) = p(b, \theta, z, t) , \quad (30)$$

where $\sigma_{rr}(a, b; \theta, z, t)$ is the normal radial stress, $\epsilon_{rr}(a, b; \theta, z, t)$ is the normal radial strain, $\epsilon_{\theta\theta}(a, b; \theta, z, t)$ is the normal circumferential strain, $\epsilon_{zz}(a, b; \theta, z, t)$ is the normal longitudinal strain, $p(a, b; \theta, z, t)$ is the external pressure on the shell in the radial direction, and a and b denote the inner and outer radius, respectively. The shear stress, strain, and longitudinal forces are related using

$$\sigma_{rz}(a, \theta, z, t) = 2\mu\epsilon_{rz}(a, \theta, z, t) = f(a, \theta, z, t) \quad (31)$$

and

$$\sigma_{rz}(b, \theta, z, t) = 2\mu\epsilon_{rz}(b, \theta, z, t) = f(b, \theta, z, t) , \quad (32)$$

where $\sigma_{rz}(a, b; \theta, z, t)$ is the shear stress, $\epsilon_{rz}(a, b; \theta, z, t)$ is the shear strain, and $f(a, b; \theta, z, t)$ is the external shear stress on the shell in the longitudinal direction.

The strains are related to the displacements in an axisymmetric solid by (Timoshenko and Goodier, 1934)

$$\epsilon_{rr} = \frac{\partial u_r}{\partial r} , \quad (33)$$

$$\epsilon_{\theta\theta} = \frac{u_r}{r} , \quad (34)$$

$$\epsilon_{zz} = \frac{\partial u_z}{\partial z} , \quad (35)$$

and

$$\epsilon_{rz} = \frac{1}{2} \left(\frac{\partial u_z}{\partial r} + \frac{\partial u_r}{\partial z} \right). \quad (36)$$

The relationship between the displacements (and the derivatives of the displacements) and the potential functions g and h_θ is found by combining equations (9), (11), (16), and (18) to produce

$$u_r = \left(\frac{dg(r)}{dr} - ikh_\theta(r) \right) e^{ikz} e^{i\omega t}, \quad (37)$$

$$u_z = \left(ikg(r) + \frac{h_\theta(r)}{r} + \frac{dh_\theta(r)}{dr} \right) e^{ikz} e^{i\omega t}, \quad (38)$$

$$\frac{\partial u_r}{\partial r} = \left(\frac{d^2g(r)}{dr^2} - ik \frac{dh_\theta(r)}{dr} \right) e^{ikz} e^{i\omega t}, \quad (39)$$

$$\frac{\partial u_z}{\partial z} = \left(-k^2 g(r) + \frac{ikh_\theta(r)}{r} + ik \frac{dh_\theta(r)}{dr} \right) e^{ikz} e^{i\omega t}, \quad (40)$$

$$\frac{\partial u_z}{\partial r} = \left(ik \frac{dg(r)}{dr} + \frac{1}{r} \frac{dh_\theta(r)}{dr} - \frac{h_\theta(r)}{r^2} + \frac{d^2h_\theta(r)}{dr^2} \right) e^{ikz} e^{i\omega t}, \quad (41)$$

and

$$\frac{\partial u_r}{\partial z} = \left(ik \frac{dg(r)}{dr} + k^2 h_\theta(r) \right) e^{ikz} e^{i\omega t}. \quad (42)$$

Combining equations (29), (30), (33), (34), (35), (37), (39), and (40) yields the normal stress in terms of the potential functions g and h_θ at $r = a$ and $r = b$. These equations are

$$(\lambda + 2\mu) \frac{d^2g(a)}{dr^2} + \frac{\lambda}{a} \frac{dg(a)}{dr} - \lambda k^2 g(a) - 2\mu ik \frac{d^2h_\theta(a)}{dr^2} = P_a \quad (43)$$

and

$$(\lambda + 2\mu) \frac{d^2g(b)}{dr^2} + \frac{\lambda}{b} \frac{dg(b)}{dr} - \lambda k^2 g(b) - 2\mu ik \frac{d^2h_\theta(b)}{dr^2} = P_b, \quad (44)$$

where P_a is the magnitude of the normal force acting on the interior of the shell and P_b is the magnitude of the normal force acting on the exterior of the shell. Combining equations (31),

(32), (36), (41), and (42) yields the shear stress in terms of the potential functions g and h_θ at $r = a$ and $r = b$. The results are

$$2\mu ik \frac{dg(a)}{dr} + \left(\mu k^2 - \frac{\mu}{a^2} \right) h_\theta(a) + \frac{\mu}{a} \frac{dh_\theta(a)}{dr} + \mu \frac{d^2 h_\theta(a)}{dr^2} = F_a \quad (45)$$

and

$$2\mu ik \frac{dg(b)}{dr} + \left(\mu k^2 - \frac{\mu}{b^2} \right) h_\theta(b) + \frac{\mu}{b} \frac{dh_\theta(b)}{dr} + \mu \frac{d^2 h_\theta(b)}{dr^2} = F_b , \quad (46)$$

where F_a is the magnitude of the (externally applied) shear stress acting on the interior of the shell and F_b is the magnitude of the (externally applied) shear stress acting on the exterior of the shell. Implicit in equations (43)-(46) is the assumption that the external loads on the shell are occurring at a definite frequency and wavenumber.

Inserting equations (25), (27), and (A-1)-(A-12) from the appendix into equations (43)-(46) and then rewriting as a four-by-four system of linear equations results in

$$\begin{bmatrix} a_{11} & a_{12} & a_{13} & a_{14} \\ a_{21} & a_{22} & a_{23} & a_{24} \\ a_{31} & a_{32} & a_{33} & a_{34} \\ a_{41} & a_{42} & a_{43} & a_{44} \end{bmatrix} \begin{Bmatrix} C_1 \\ C_2 \\ C_3 \\ C_4 \end{Bmatrix} = \begin{Bmatrix} P_a \\ P_b \\ F_a \\ F_b \end{Bmatrix} , \quad (47)$$

where the matrix coefficients a_{nm} are determined by the magnitude of the wavenumber k . In the low-wavenumber region,

$$|k| < \frac{\omega}{c_d} < \frac{\omega}{c_s} , \quad (48)$$

and the matrix coefficients are

$$a_{11} = \left[(-\lambda - 2\mu) \left(\frac{\alpha^2}{2} \right) - \lambda k^2 \right] J_0(\alpha a) + \left(\frac{-\lambda \alpha}{a} \right) J_1(\alpha a) + (\lambda + 2\mu) \left(\frac{\alpha^2}{2} \right) J_2(\alpha a) , \quad (49)$$

$$a_{12} = \left[(-\lambda - 2\mu) \left(\frac{\alpha^2}{2} \right) - \lambda k^2 \right] Y_0(\alpha a) + \left(\frac{-\lambda \alpha}{a} \right) Y_1(\alpha a) + (\lambda + 2\mu) \left(\frac{\alpha^2}{2} \right) Y_2(\alpha a) , \quad (50)$$

$$a_{13} = (-i\mu k \beta) J_0(\beta a) + (i\mu k \beta) J_2(\beta a) , \quad (51)$$

$$a_{14} = (-i\mu k\beta)Y_0(\beta a) + (i\mu k\beta)Y_2(\beta a) , \quad (52)$$

$$a_{21} = \left[(-\lambda - 2\mu) \left(\frac{\alpha^2}{2} \right) - \lambda k^2 \right] J_0(\alpha b) + \left(\frac{-\lambda \alpha}{b} \right) J_1(\alpha b) + (\lambda + 2\mu) \left(\frac{\alpha^2}{2} \right) J_2(\alpha b) , \quad (53)$$

$$a_{22} = \left[(-\lambda - 2\mu) \left(\frac{\alpha^2}{2} \right) - \lambda k^2 \right] Y_0(\alpha b) + \left(\frac{-\lambda \alpha}{b} \right) Y_1(\alpha b) + (\lambda + 2\mu) \left(\frac{\alpha^2}{2} \right) Y_2(\alpha b) , \quad (54)$$

$$a_{23} = (-i\mu k\beta)J_0(\beta b) + (i\mu k\beta)J_2(\beta b) , \quad (55)$$

$$a_{24} = (-i\mu k\beta)Y_0(\beta b) + (i\mu k\beta)Y_2(\beta b) , \quad (56)$$

$$a_{31} = (-i2\mu k\alpha)J_1(\alpha a) , \quad (57)$$

$$a_{32} = (-i2\mu k\alpha)Y_1(\alpha a) , \quad (58)$$

$$a_{33} = \left(\frac{\mu\beta}{2a} \right) J_0(\beta a) + \left(\mu k^2 - \frac{\mu}{a^2} - \frac{3\mu\beta^2}{4} \right) J_1(\beta a) + \left(\frac{-\mu\beta}{2a} \right) J_2(\beta a) + \left(\frac{\mu\beta^2}{4} \right) J_3(\beta a) , \quad (59)$$

$$a_{34} = \left(\frac{\mu\beta}{2a} \right) Y_0(\beta a) + \left(\mu k^2 - \frac{\mu}{a^2} - \frac{3\mu\beta^2}{4} \right) Y_1(\beta a) + \left(\frac{-\mu\beta}{2a} \right) Y_2(\beta a) + \left(\frac{\mu\beta^2}{4} \right) Y_3(\beta a) , \quad (60)$$

$$a_{41} = (-i2\mu k\alpha)J_1(\alpha b) , \quad (61)$$

$$a_{42} = (-i2\mu k\alpha)Y_1(\alpha b) , \quad (62)$$

$$a_{43} = \left(\frac{\mu\beta}{2b} \right) J_0(\beta b) + \left(\mu k^2 - \frac{\mu}{b^2} - \frac{3\mu\beta^2}{4} \right) J_1(\beta b) + \left(\frac{-\mu\beta}{2b} \right) J_2(\beta b) + \left(\frac{\mu\beta^2}{4} \right) J_3(\beta b) , \quad (63)$$

and

$$a_{44} = \left(\frac{\mu\beta}{2b} \right) Y_0(\beta b) + \left(\mu k^2 - \frac{\mu}{b^2} - \frac{3\mu\beta^2}{4} \right) Y_1(\beta b) + \left(\frac{-\mu\beta}{2b} \right) Y_2(\beta b) + \left(\frac{\mu\beta^2}{4} \right) Y_3(\beta b) . \quad (64)$$

In the medium-wavenumber region,

$$\frac{\omega}{c_d} < |k| < \frac{\omega}{c_s} , \quad (65)$$

and the matrix coefficients are

$$a_{11} = \left[(\lambda + 2\mu) \left(\frac{\alpha^2}{2} \right) - \lambda k^2 \right] I_0(\alpha a) + \left(\frac{\lambda \alpha}{a} \right) I_1(\alpha a) + (\lambda + 2\mu) \left(\frac{\alpha^2}{2} \right) I_2(\alpha a) , \quad (66)$$

$$a_{12} = \left[(\lambda + 2\mu) \left(\frac{\alpha^2}{2} \right) - \lambda k^2 \right] K_0(\alpha a) + \left(\frac{-\lambda \alpha}{a} \right) K_1(\alpha a) + (\lambda + 2\mu) \left(\frac{\alpha^2}{2} \right) K_2(\alpha a) , \quad (67)$$

$$a_{13} = (-i\mu k \beta) J_0(\beta a) + (i\mu k \beta) J_2(\beta a) , \quad (68)$$

$$a_{14} = (-i\mu k \beta) Y_0(\beta a) + (i\mu k \beta) Y_2(\beta a) , \quad (69)$$

$$a_{21} = \left[(\lambda + 2\mu) \left(\frac{\alpha^2}{2} \right) - \lambda k^2 \right] I_0(\alpha b) + \left(\frac{\lambda \alpha}{b} \right) I_1(\alpha b) + (\lambda + 2\mu) \left(\frac{\alpha^2}{2} \right) I_2(\alpha b) , \quad (70)$$

$$a_{22} = \left[(\lambda + 2\mu) \left(\frac{\alpha^2}{2} \right) - \lambda k^2 \right] K_0(\alpha b) + \left(\frac{-\lambda \alpha}{b} \right) K_1(\alpha b) + (\lambda + 2\mu) \left(\frac{\alpha^2}{2} \right) K_2(\alpha b) , \quad (71)$$

$$a_{23} = (-i\mu k \beta) J_0(\beta b) + (i\mu k \beta) J_2(\beta b) , \quad (72)$$

$$a_{24} = (-i\mu k \beta) Y_0(\beta b) + (i\mu k \beta) Y_2(\beta b) , \quad (73)$$

$$a_{31} = (i2\mu k \alpha) I_1(\alpha a) , \quad (74)$$

$$a_{32} = (-i2\mu k \alpha) K_1(\alpha a) , \quad (75)$$

$$a_{33} = \left(\frac{\mu \beta}{2a} \right) J_0(\beta a) + \left(\mu k^2 - \frac{\mu}{a^2} - \frac{3\mu \beta^2}{4} \right) J_1(\beta a) + \left(\frac{-\mu \beta}{2a} \right) J_2(\beta a) + \left(\frac{\mu \beta^2}{4} \right) J_3(\beta a) , \quad (76)$$

$$a_{34} = \left(\frac{\mu \beta}{2a} \right) Y_0(\beta a) + \left(\mu k^2 - \frac{\mu}{a^2} - \frac{3\mu \beta^2}{4} \right) Y_1(\beta a) + \left(\frac{-\mu \beta}{2a} \right) Y_2(\beta a) + \left(\frac{\mu \beta^2}{4} \right) Y_3(\beta a) , \quad (77)$$

$$a_{41} = (i2\mu k \alpha) I_1(\alpha b) , \quad (78)$$

$$a_{42} = (-i2\mu k \alpha) K_1(\alpha b) , \quad (79)$$

$$a_{43} = \left(\frac{\mu \beta}{2b} \right) J_0(\beta b) + \left(\mu k^2 - \frac{\mu}{b^2} - \frac{3\mu \beta^2}{4} \right) J_1(\beta b) + \left(\frac{-\mu \beta}{2b} \right) J_2(\beta b) + \left(\frac{\mu \beta^2}{4} \right) J_3(\beta b) , \quad (80)$$

and

$$a_{44} = \left(\frac{\mu\beta}{2b} \right) Y_0(\beta b) + \left(\mu k^2 - \frac{\mu}{b^2} - \frac{3\mu\beta^2}{4} \right) Y_1(\beta b) + \left(\frac{-\mu\beta}{2b} \right) Y_2(\beta b) + \left(\frac{\mu\beta^2}{4} \right) Y_3(\beta b) . \quad (81)$$

In the high-wavenumber region,

$$\frac{\omega}{c_d} < \frac{\omega}{c_s} < |k| , \quad (82)$$

and the matrix coefficients are

$$a_{11} = \left[(\lambda + 2\mu) \left(\frac{\alpha^2}{2} \right) - \lambda k^2 \right] I_0(\alpha a) + \left(\frac{\lambda \alpha}{a} \right) I_1(\alpha a) + (\lambda + 2\mu) \left(\frac{\alpha^2}{2} \right) I_2(\alpha a) , \quad (83)$$

$$a_{12} = \left[(\lambda + 2\mu) \left(\frac{\alpha^2}{2} \right) - \lambda k^2 \right] K_0(\alpha a) + \left(\frac{-\lambda \alpha}{a} \right) K_1(\alpha a) + (\lambda + 2\mu) \left(\frac{\alpha^2}{2} \right) K_2(\alpha a) , \quad (84)$$

$$a_{13} = (-i\mu k \beta) I_0(\beta a) + (-i\mu k \beta) I_2(\beta a) , \quad (85)$$

$$a_{14} = (i\mu k \beta) K_0(\beta a) + (i\mu k \beta) K_2(\beta a) , \quad (86)$$

$$a_{21} = \left[(\lambda + 2\mu) \left(\frac{\alpha^2}{2} \right) - \lambda k^2 \right] I_0(\alpha b) + \left(\frac{\lambda \alpha}{b} \right) I_1(\alpha b) + (\lambda + 2\mu) \left(\frac{\alpha^2}{2} \right) I_2(\alpha b) , \quad (87)$$

$$a_{22} = \left[(\lambda + 2\mu) \left(\frac{\alpha^2}{2} \right) - \lambda k^2 \right] K_0(\alpha b) + \left(\frac{-\lambda \alpha}{b} \right) K_1(\alpha b) + (\lambda + 2\mu) \left(\frac{\alpha^2}{2} \right) K_2(\alpha b) , \quad (88)$$

$$a_{23} = (-i\mu k \beta) I_0(\beta b) + (-i\mu k \beta) I_2(\beta b) , \quad (89)$$

$$a_{24} = (i\mu k \beta) K_0(\beta b) + (i\mu k \beta) K_2(\beta b) , \quad (90)$$

$$a_{31} = (i2\mu k \alpha) I_1(\alpha a) , \quad (91)$$

$$a_{32} = (-i2\mu k \alpha) K_1(\alpha a) , \quad (92)$$

$$a_{33} = \left(\frac{\mu\beta}{2a} \right) I_0(\beta a) + \left(\mu k^2 - \frac{\mu}{a^2} + \frac{3\mu\beta^2}{4} \right) I_1(\beta a) + \left(\frac{\mu\beta}{2a} \right) I_2(\beta a) + \left(\frac{\mu\beta^2}{4} \right) I_3(\beta a) , \quad (93)$$

$$a_{34} = \left(\frac{-\mu\beta}{2a} \right) K_0(\beta a) + \left(\mu k^2 - \frac{\mu}{a^2} + \frac{3\mu\beta^2}{4} \right) K_1(\beta a) + \left(\frac{-\mu\beta}{2a} \right) K_2(\beta a) + \left(\frac{\mu\beta^2}{4} \right) K_3(\beta a) , \quad (94)$$

$$a_{41} = (i2\mu k \alpha) I_1(\alpha b) , \quad (95)$$

$$a_{42} = (-i2\mu k\alpha)K_1(\alpha b) , \quad (96)$$

$$a_{43} = \left(\frac{\mu\beta}{2b}\right)I_0(\beta b) + \left(\mu k^2 - \frac{\mu}{b^2} + \frac{3\mu\beta^2}{4}\right)I_1(\beta b) + \left(\frac{\mu\beta}{2b}\right)I_2(\beta b) + \left(\frac{\mu\beta^2}{4}\right)I_3(\beta b) , \quad (97)$$

and

$$a_{44} = \left(\frac{-\mu\beta}{2b}\right)K_0(\beta b) + \left(\mu k^2 - \frac{\mu}{b^2} + \frac{3\mu\beta^2}{4}\right)K_1(\beta b) + \left(\frac{-\mu\beta}{2b}\right)K_2(\beta b) + \left(\frac{\mu\beta^2}{4}\right)K_3(\beta b) . \quad (98)$$

Finally, the displacements of the forced system can be determined by use of the constants C_1 , C_2 , C_3 , and C_4 in the low-wavenumber region as

$$u_r = [-C_1\alpha J_1(\alpha r) - C_2\alpha Y_1(\alpha r) - C_3ikJ_1(\beta r) - C_4ikY_1(\beta r)] e^{ikx} e^{i\omega t} \quad (99)$$

and

$$\begin{aligned} u_z = & \{ C_1ikJ_0(\alpha r) + C_2ikY_0(\alpha r) \\ & + C_3 \left[\left(\frac{\beta}{2}\right)J_0(\beta r) + \left(\frac{1}{r}\right)J_1(\beta r) - \left(\frac{\beta}{2}\right)J_2(\beta r) \right] \\ & + C_4 \left[\left(\frac{\beta}{2}\right)Y_0(\beta r) + \left(\frac{1}{r}\right)Y_1(\beta r) - \left(\frac{\beta}{2}\right)Y_2(\beta r) \right] \} e^{ikx} e^{i\omega t} ; \end{aligned} \quad (100)$$

in the medium-wavenumber region as

$$u_r = [C_1\alpha I_1(\alpha r) - C_2\alpha K_1(\alpha r) - C_3ikJ_1(\beta r) - C_4ikY_1(\beta r)] e^{ikx} e^{i\omega t} \quad (101)$$

and

$$\begin{aligned} u_z = & \{ C_1ikI_0(\alpha r) + C_2ikK_0(\alpha r) \\ & + C_3 \left[\left(\frac{\beta}{2}\right)J_0(\beta r) + \left(\frac{1}{r}\right)J_1(\beta r) - \left(\frac{\beta}{2}\right)J_2(\beta r) \right] \\ & + C_4 \left[\left(\frac{\beta}{2}\right)Y_0(\beta r) + \left(\frac{1}{r}\right)Y_1(\beta r) - \left(\frac{\beta}{2}\right)Y_2(\beta r) \right] \} e^{ikx} e^{i\omega t} ; \end{aligned} \quad (102)$$

and in the high-wavenumber region as

$$u_r = [C_1 \alpha I_1(\alpha r) - C_2 \alpha K_1(\alpha r) - C_3 i k I_1(\beta r) - C_4 i k K_1(\beta r)] e^{i k x} e^{i \omega t} \quad (103)$$

and

$$\begin{aligned} u_z = & \{ C_1 i k I_0(\alpha r) + C_2 i k K_0(\alpha r) \\ & + C_3 \left[\left(\frac{\beta}{2} \right) I_0(\beta r) + \left(\frac{1}{r} \right) I_1(\beta r) + \left(\frac{\beta}{2} \right) I_2(\beta r) \right] \\ & + C_4 \left[\left(\frac{-\beta}{2} \right) K_0(\beta r) + \left(\frac{1}{r} \right) K_1(\beta r) - \left(\frac{\beta}{2} \right) K_2(\beta r) \right] \} e^{i k x} e^{i \omega t} . \end{aligned} \quad (104)$$

Equations (99), (101), and (103) can be written as

$$u_r = U_r(r) e^{i k z} e^{i \omega t} , \quad (105)$$

and equations (100), (102), and (104) can be expressed as

$$u_z = U_z(r) e^{i k z} e^{i \omega t} . \quad (106)$$

3. MODEL VALIDATION

The new thick shell model is validated by comparing it to a thin shell problem. The thickness of the thick shell model is set to a very small value (relative to the shell radius) to ensure such an accurate comparison. The governing partial differential equations for an axisymmetric, isotropic thin shell are (Hull, 1994)

$$\rho h \frac{\partial^2 u_z(z,t)}{\partial t^2} = h E_x \frac{\partial^2 u_z(z,t)}{\partial z^2} + \frac{\nu h E_x}{a} \frac{\partial u_r(z,t)}{\partial z} + f(z,t) \quad (107)$$

and

$$\rho h \frac{\partial^2 u_r(z,t)}{\partial t^2} = -\frac{h^3 E_x}{12} \frac{\partial^4 u_r(z,t)}{\partial z^4} - \frac{h E_x}{a^2} u_r(z,t) - \frac{\nu h E_x}{a} \frac{\partial u_z(z,t)}{\partial z} - p(z,t) , \quad (108)$$

where E_x is the effective modulus of elasticity, ν is Poisson's ratio, a is the mean radius of the shell, and h is its thickness. The relationship between the effective modulus and Young's modulus is given by

$$E_x = \frac{E}{1 - \nu^2} , \quad (109)$$

where E is Young's modulus. The definition of the Lamé constants (from section 2) in terms of material properties (Young's modulus E and Poisson's ratio ν) are (Mirsky and Herrmann, 1958)

$$\lambda = \frac{\nu E}{(1 + \nu)(1 - 2\nu)} \quad (110)$$

and

$$\mu = \frac{E}{2(1 + \nu)} . \quad (111)$$

Equations (107) and (108) are solved as an infinite length system by setting the displacements and forcing functions at a specific wavenumber and frequency, resulting in the following equations:

$$u_r(x, t) = U_r e^{ikx} e^{i\omega t} , \quad (112)$$

$$u_z(x, t) = U_z e^{ikx} e^{i\omega t} , \quad (113)$$

$$f(x, t) = F e^{ikx} e^{i\omega t} , \quad (114)$$

and

$$p(x, t) = P e^{ikx} e^{i\omega t} . \quad (115)$$

Inserting the values and derivatives of equations (112)-(115) into equations (107) and (108) produces a two-by-two system of linear algebraic equations:

$$\begin{bmatrix} b_{11} & b_{12} \\ b_{21} & b_{22} \end{bmatrix} \begin{Bmatrix} U_z \\ U_r \end{Bmatrix} = \begin{Bmatrix} F \\ P \end{Bmatrix} , \quad (116)$$

where

$$b_{11} = hE_x k^2 - h\rho\omega^2, \quad (117)$$

$$b_{12} = \frac{-ikh\nu E_x}{a}, \quad (118)$$

$$b_{21} = \frac{-ikh\nu E_x}{a}, \quad (119)$$

and

$$b_{22} = \rho h\omega^2 - \frac{hE_x}{a^2} - \frac{h^3 E_x k^4}{12}. \quad (120)$$

Note that both U_r and U_z are constant with respect to r for the thin shell equations of motion.

Figures 3-6 show the transfer functions of displacements divided by forcing functions for a shell with a mean radius of 0.1 m, thickness of 0.001 m, Poisson's ratio of 0.4 (dimensionless), Young's modulus of 1×10^9 N/m², density of 2000 kg/m³, and frequency of 50 Hz. The ratio of thickness to radius (h/a) is 1/100. The corresponding dilatational wave speed is 1035.1 m/s and the corresponding shear wave speed is 422.6 m/s. In these figures, the solid line represents the thick shell model and the X's denote the thin shell model. Figure 3 plots the magnitude of the axial displacement divided by applied axial stress versus wavenumber, and figure 4 plots the magnitude of the radial displacement divided by applied axial stress versus wavenumber. In both figures, the applied radial pressure on the shell was set equal to zero. Figure 5 is a plot of the magnitude of the axial displacement divided by applied radial pressure versus wavenumber, and figure 6 is a plot of the magnitude of the radial displacement divided by applied radial pressure versus wavenumber. In both figures, the applied axial stress on the shell was set equal to zero. All the figures show the thick shell model to be in agreement with the thin shell model. Because the figures are symmetric in wavenumber, the negative wavenumbers are not shown. The thick shell forcing functions were applied to the exterior of the thick shell model. Identical results would be obtained by application of the loads to the interior of the thick shell because the shell thickness in this example is set to such a small value.

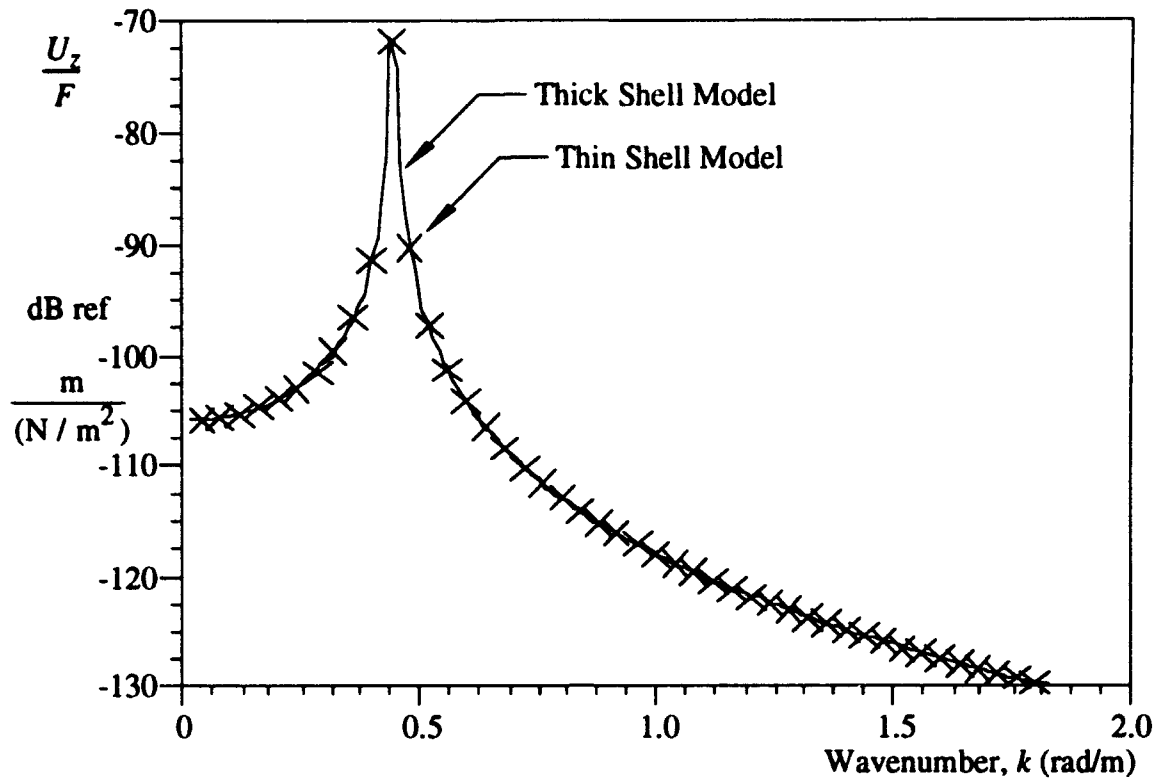


Figure 3. Magnitude of Axial Displacement Divided by Applied Axial Stress: Comparison of Thick Shell Model to Thin Shell Model, $f = 50$ Hz, $h/a = 1/100$

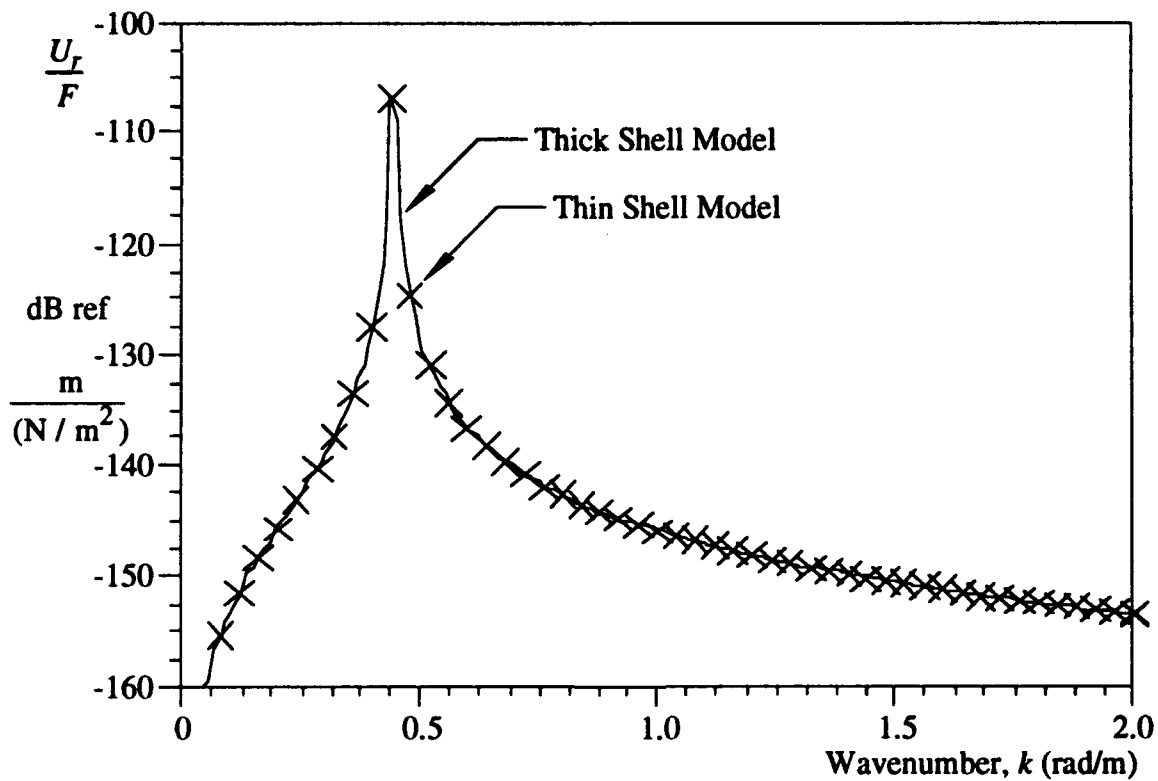


Figure 4. Magnitude of Radial Displacement Divided by Applied Axial Stress: Comparison of Thick Shell Model to Thin Shell Model, $f = 50$ Hz, $h/a = 1/100$

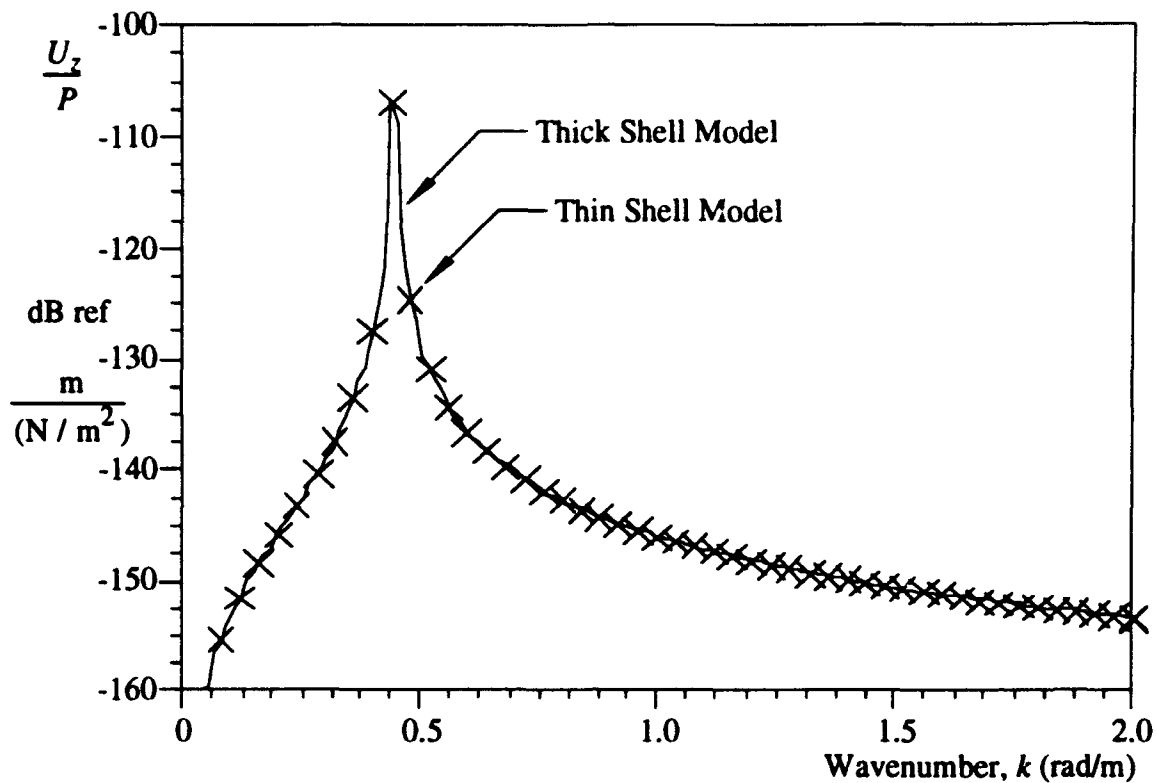


Figure 5. Magnitude of Axial Displacement Divided by Applied Radial Pressure: Comparison of Thick Shell Model to Thin Shell Model, $f = 50$ Hz, $h/a = 1/100$

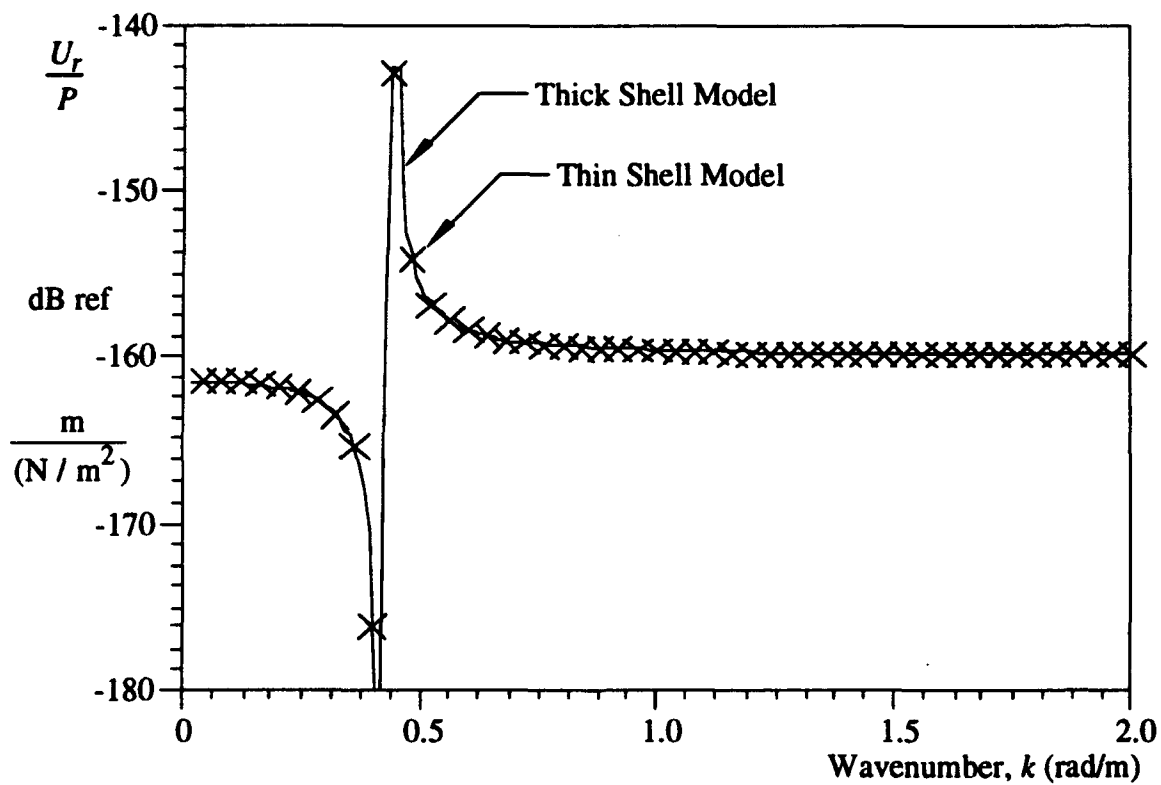


Figure 6. Magnitude of Radial Displacement Divided by Applied Radial Pressure: Comparison of Thick Shell Model to Thin Shell Model, $f = 50$ Hz, $h/a = 1/100$

4. ANALYSIS

The thick shell model is now investigated for a shell whose thickness to mean radius ratio $[(2h/(a+b))]$ is 1. For this example, the mean radius $[(a+b)/2]$ is 0.1 m, the inner radius (a) is 0.05 m, the outer radius (b) is 0.15 m, and the shell thickness (h) is 0.1 m. Other properties of the shell are a Poisson's ratio of 0.4 (dimensionless), a Young's modulus of $1 \times 10^9 \text{ N/m}^2$, and a density of 2000 kg/m^3 . The forcing functions were applied to the exterior of the shell at two frequencies: 50 and 500 Hz.

In figures 7-14, the thick shell model is compared to the thin shell model. The thick shell model is shown at the mean radius value of $r = (a+b)/2$ and denoted using a solid line, while the thin shell model is shown with a dashed line. Figure 7 is a comparison of the magnitude of the axial displacement divided by applied axial stress versus wavenumber, and figure 8 is a comparison of the magnitude of the radial displacement divided by applied axial stress versus wavenumber. In both figures, the applied radial pressure on the shell was set equal to zero. Figure 9 plots the magnitude of the axial displacement divided by applied radial pressure versus wavenumber, and figure 10 plots the magnitude of the radial displacement divided by applied radial pressure versus wavenumber. In both figures, the applied axial stress on the shell was set equal to zero. The analysis in figures 7-10 was computed at 50 Hz. In most of the wavenumbers shown, the thin shell model underpredicts the system response by 2 to 8 dB. Figure 11 compares the magnitude of the axial displacement divided by applied axial stress versus wavenumber, and figure 12 compares the magnitude of the radial displacement divided by applied axial stress versus wavenumber. In both figures, the applied radial pressure on the shell was set equal to zero. Figure 13 is a plot of the magnitude of the axial displacement divided by applied radial pressure versus wavenumber, and figure 14 is a plot of the magnitude of the radial displacement divided by applied radial pressure versus wavenumber. In both figures, the applied axial stress on the shell was set equal to zero. The analysis in figures 11-14 was computed at 500 Hz. Figures 11-14 show behavior at low wavenumbers similar to that shown in figures 7-10 where the thin shell theory usually

underpredicts the response. There is a crossover of the thick shell and the thin shell models at higher wavenumbers in figures 11 and 12.

In figures 15-22, the thick shell model response at the exterior of the shell ($r = b$) is compared to the thick shell model response at the interior of the shell ($r = a$). The solid line denotes the response at $r = a$ and the dashed line at $r = b$. Figure 15 compares the magnitude of the axial displacement divided by applied axial stress versus wavenumber, and figure 16 compares the magnitude of the radial displacement divided by applied axial stress versus wavenumber. Figure 17 is a plot of the magnitude of the axial displacement divided by applied radial pressure versus wavenumber, and figure 18 is a plot of the magnitude of the radial displacement divided by applied radial pressure versus wavenumber. The analysis in figures 15-18 was computed at 50 Hz. These figures correspond to figures 7-10, except the values now shown are the transfer functions at the interior and the exterior of the shell. For thin shell theory, these two transfer functions are identical (and also equal to the value at the mean radius of the shell). Note that in figure 16 these two transfer functions are significantly different. Figure 19 is a comparison of the magnitude of the axial displacement divided by applied axial stress versus wavenumber, and figure 20 is a comparison of the magnitude of the radial displacement divided by applied axial stress versus wavenumber. Figure 21 plots the magnitude of the axial displacement divided by applied radial pressure versus wavenumber, and figure 22 plots the magnitude of the radial displacement divided by applied radial pressure versus wavenumber. The analysis in figures 19-22 was computed at 500 Hz. These figures correspond to figures 11-14, except the values now shown are the transfer functions at the interior and the exterior of the shell. Note that, except for figure 22, the transfer function at the interior of the shell compared with that at the exterior of the shell is significantly different.

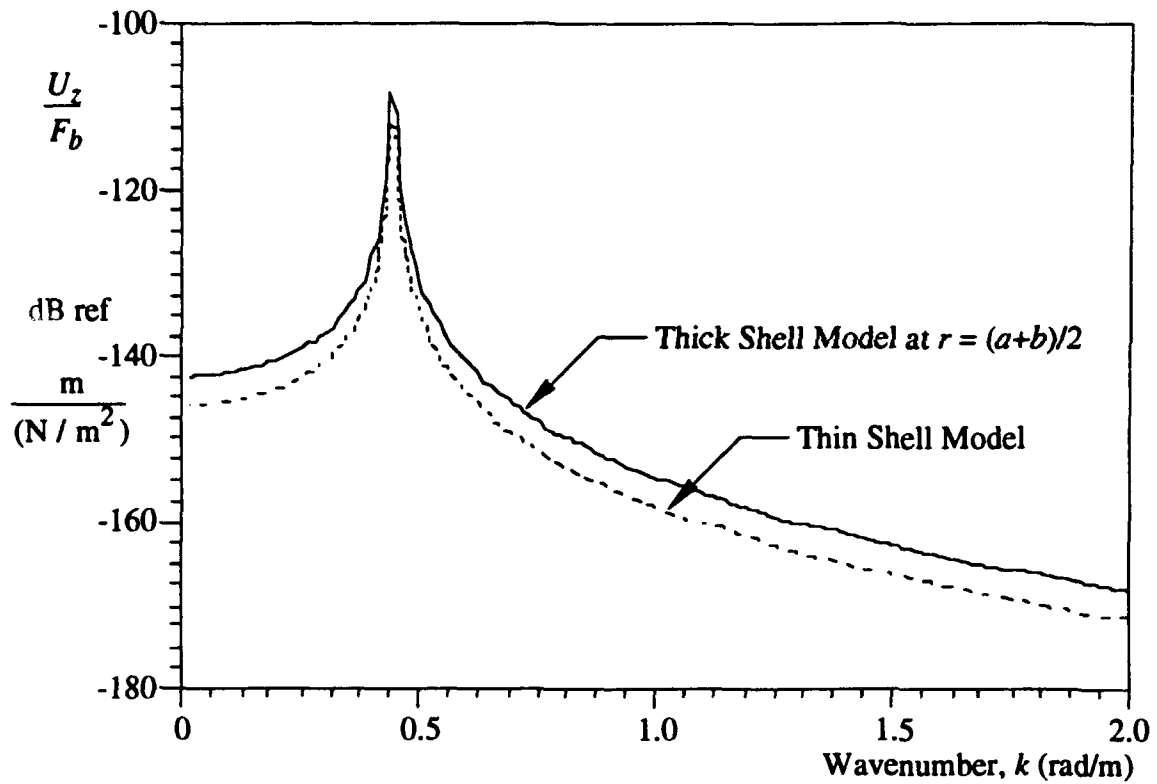


Figure 7. Magnitude of Axial Displacement Divided by Applied Axial Stress: Comparison of Thick Shell Model to Thin Shell Model, $f = 50$ Hz, $2h/(a+b) = 1$

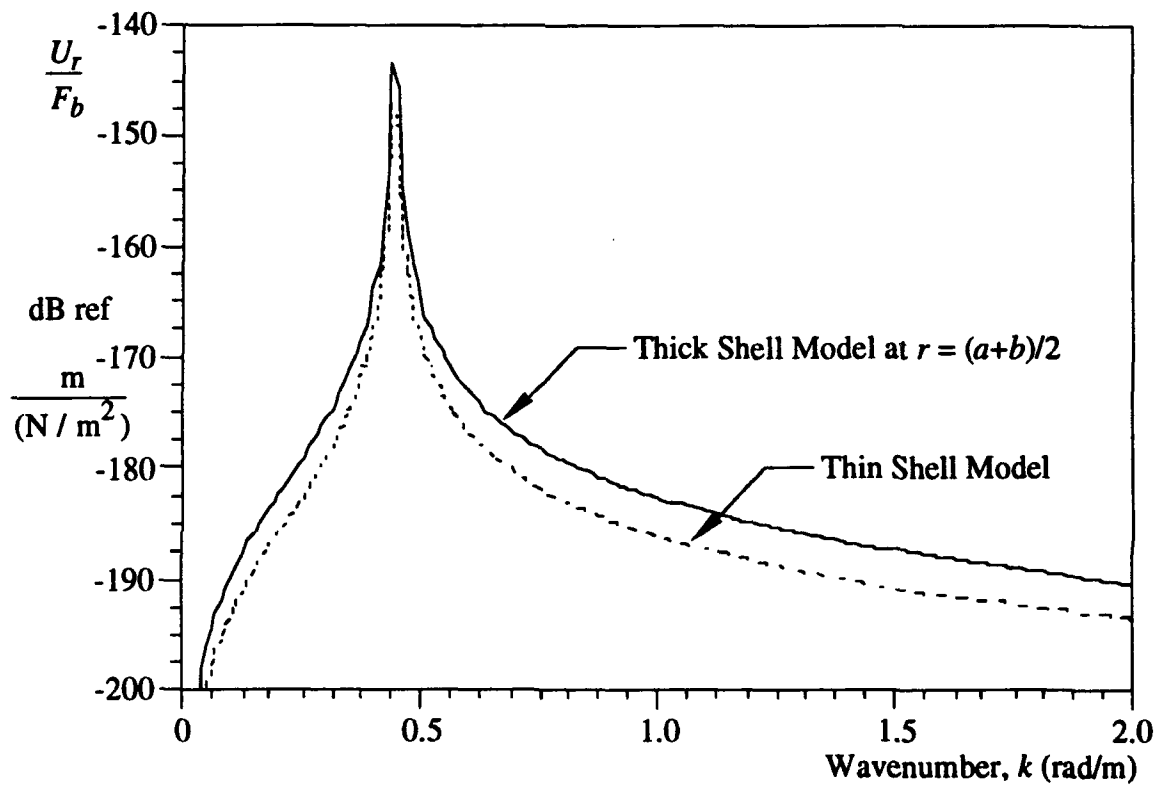


Figure 8. Magnitude of Radial Displacement Divided by Applied Axial Stress: Comparison of Thick Shell Model to Thin Shell Model, $f = 50$ Hz, $2h/(a+b) = 1$

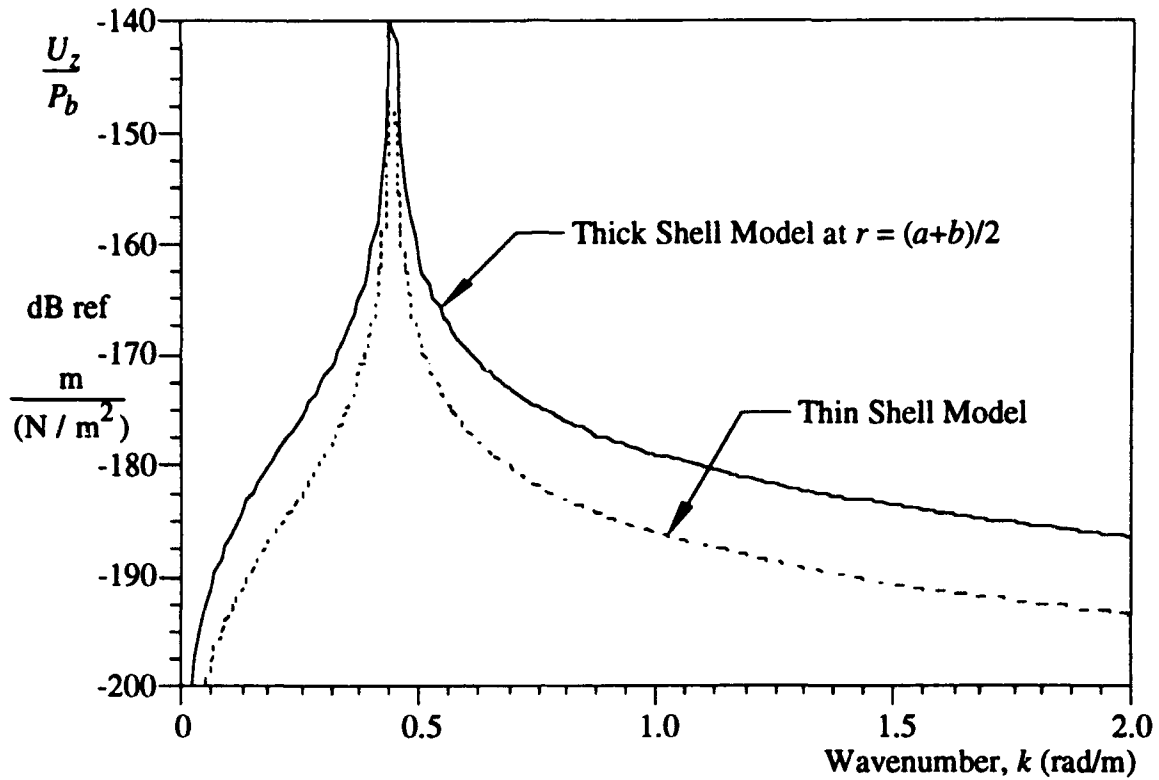


Figure 9. Magnitude of Axial Displacement Divided by Applied Radial Pressure: Comparison of Thick Shell Model to Thin Shell Model, $f = 50$ Hz, $2h/(a+b) = 1$

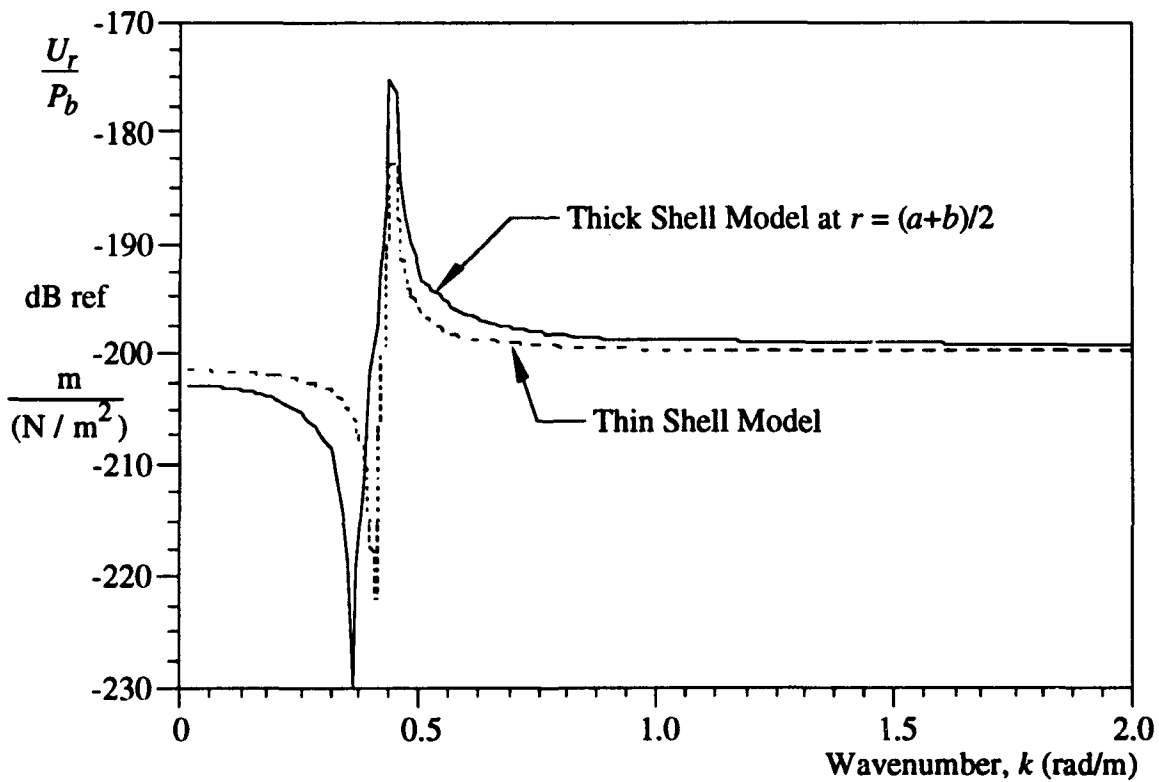


Figure 10. Magnitude of Radial Displacement Divided by Applied Radial Pressure: Comparison of Thick Shell Model to Thin Shell Model, $f = 50$ Hz, $2h/(a+b) = 1$

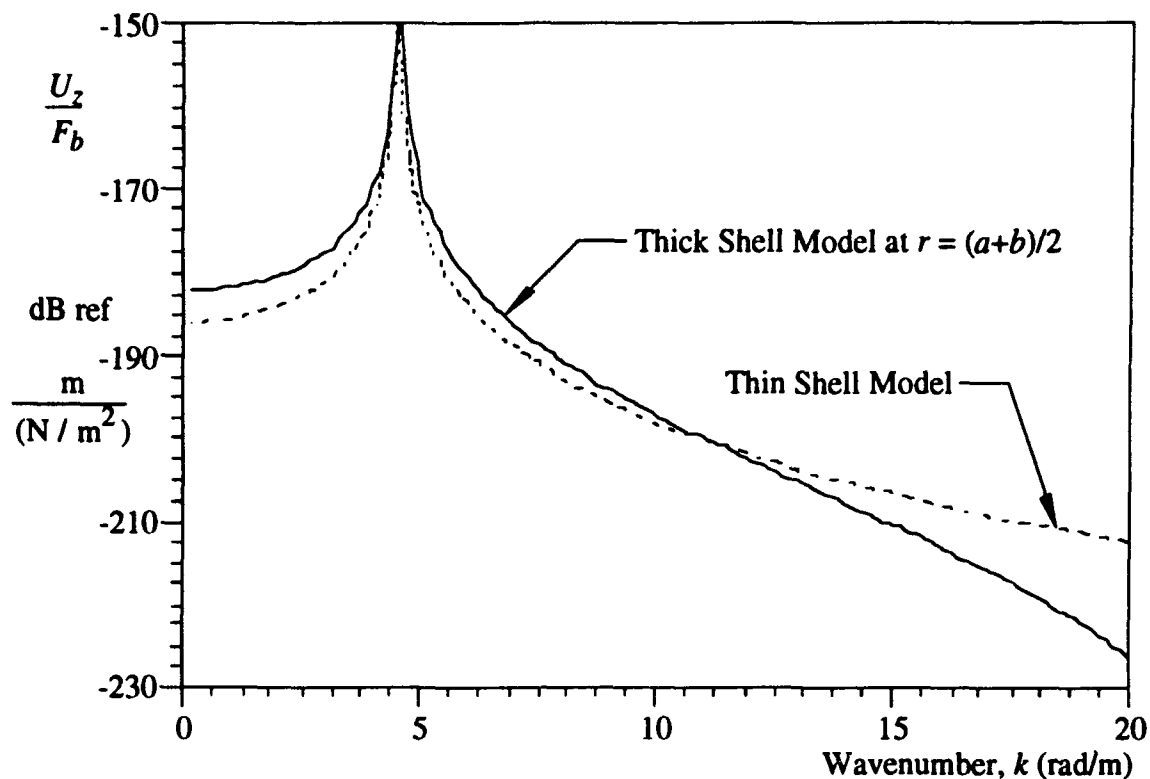


Figure 11. Magnitude of Axial Displacement Divided by Applied Axial Stress: Comparison of Thick Shell Model to Thin Shell Model, $f = 500$ Hz, $2h/(a+b) = 1$

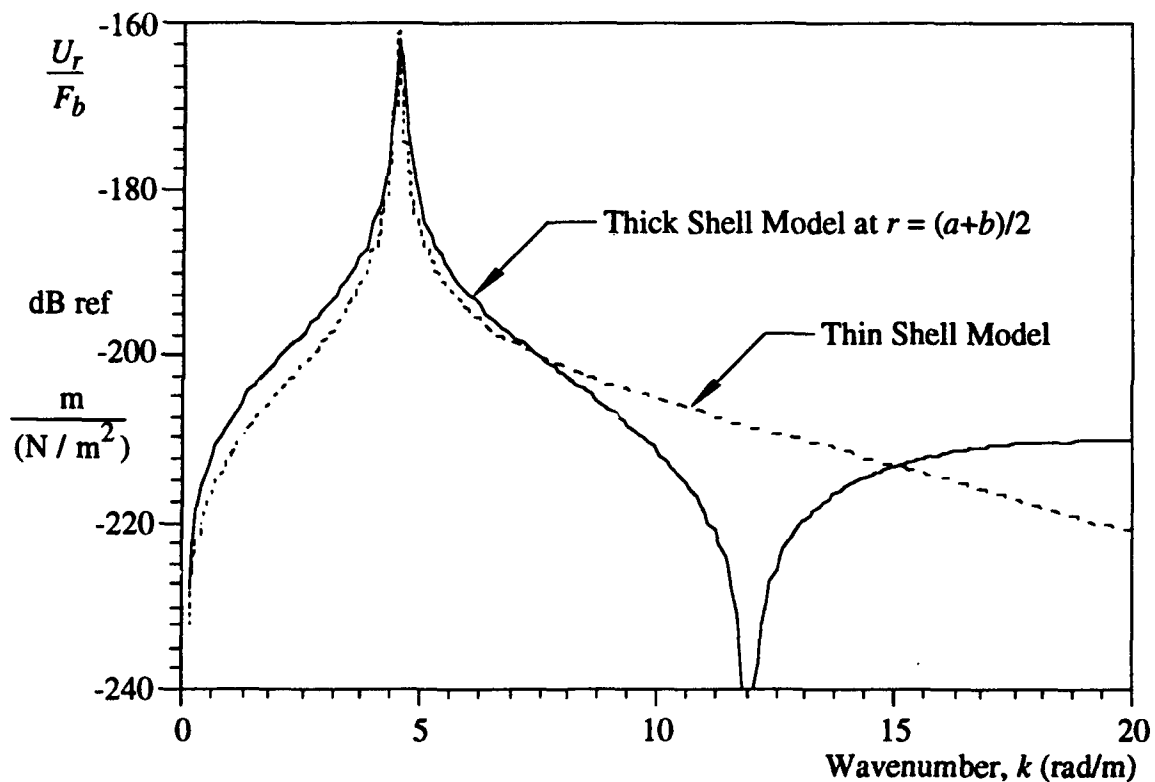


Figure 12. Magnitude of Radial Displacement Divided by Applied Axial Stress: Comparison of Thick Shell Model to Thin Shell Model, $f = 500$ Hz, $2h/(a+b) = 1$

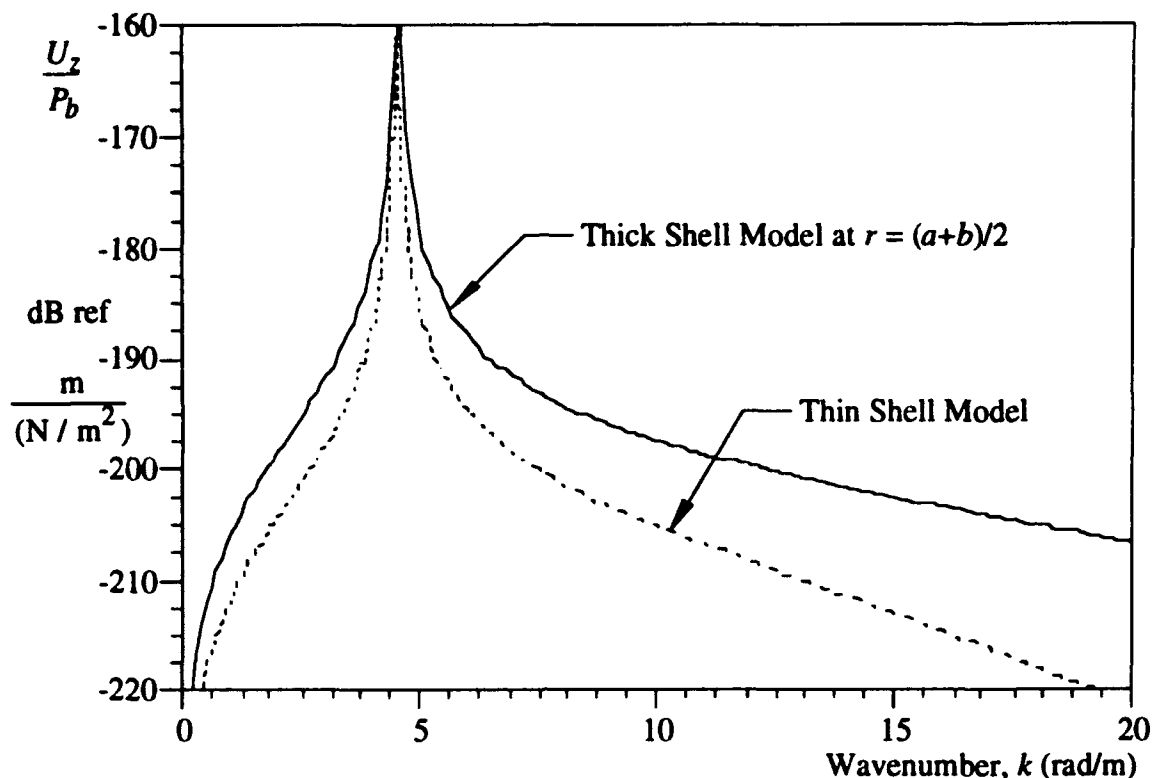


Figure 13. Magnitude of Axial Displacement Divided by Applied Radial Pressure: Comparison of Thick Shell Model to Thin Shell Model, $f = 500$ Hz, $2h/(a+b) = 1$

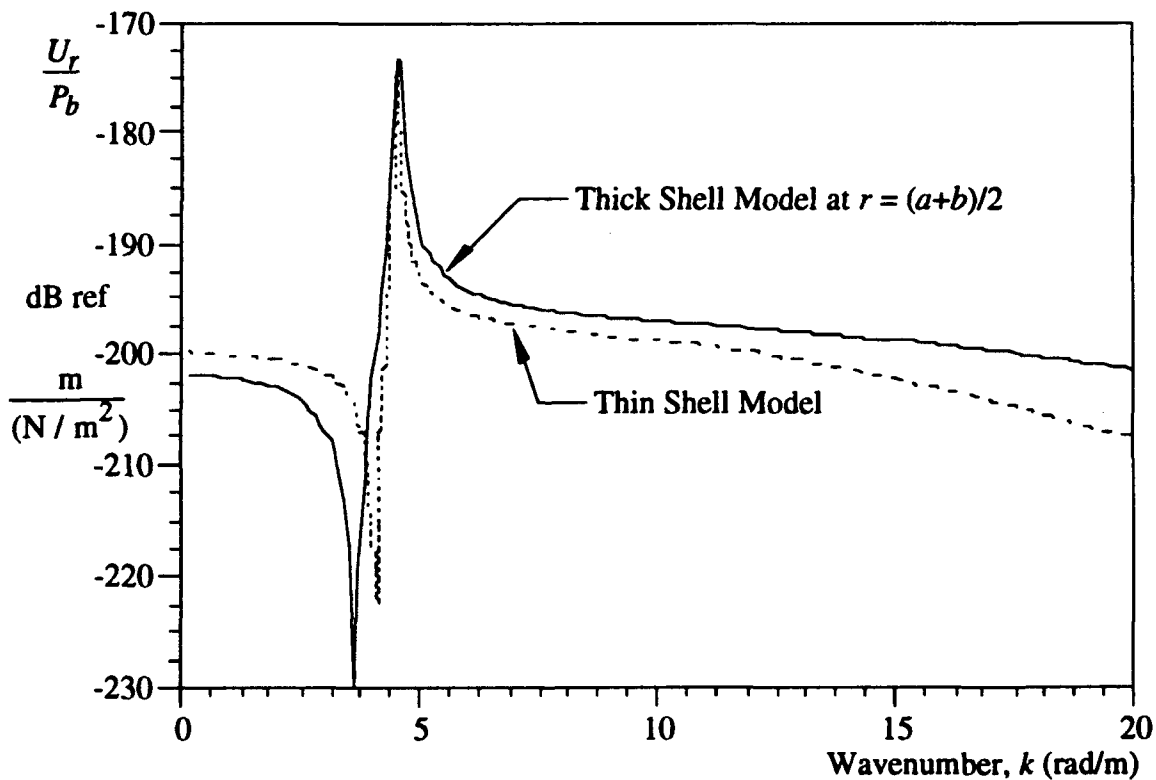


Figure 14. Magnitude of Radial Displacement Divided by Applied Radial Pressure: Comparison of Thick Shell Model to Thin Shell Model, $f = 500$ Hz, $2h/(a+b) = 1$

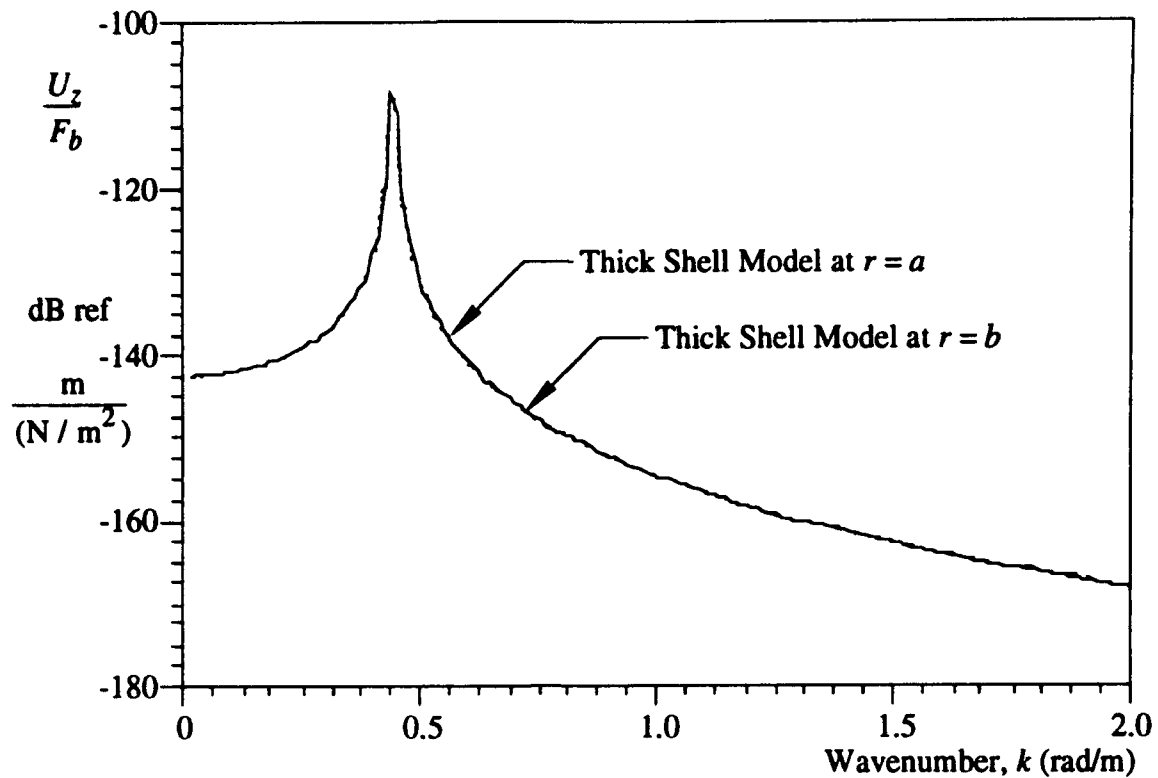


Figure 15. Magnitude of Axial Displacement Divided by Applied Axial Stress:
Comparison of Transfer Function at $r = a$ to $r = b$, $f = 50$ Hz, $2h/(a+b) = 1$

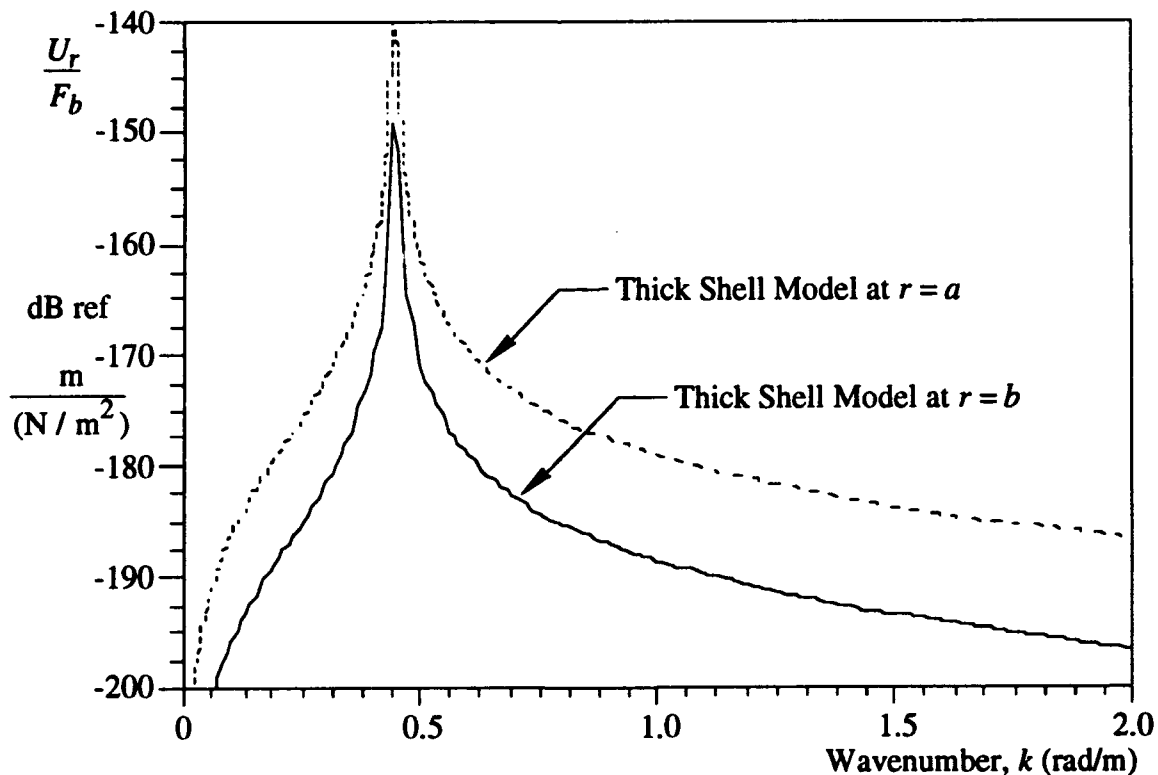


Figure 16. Magnitude of Radial Displacement Divided by Applied Axial Stress:
Comparison of Transfer Function at $r = a$ to $r = b$, $f = 50$ Hz, $2h/(a+b) = 1$

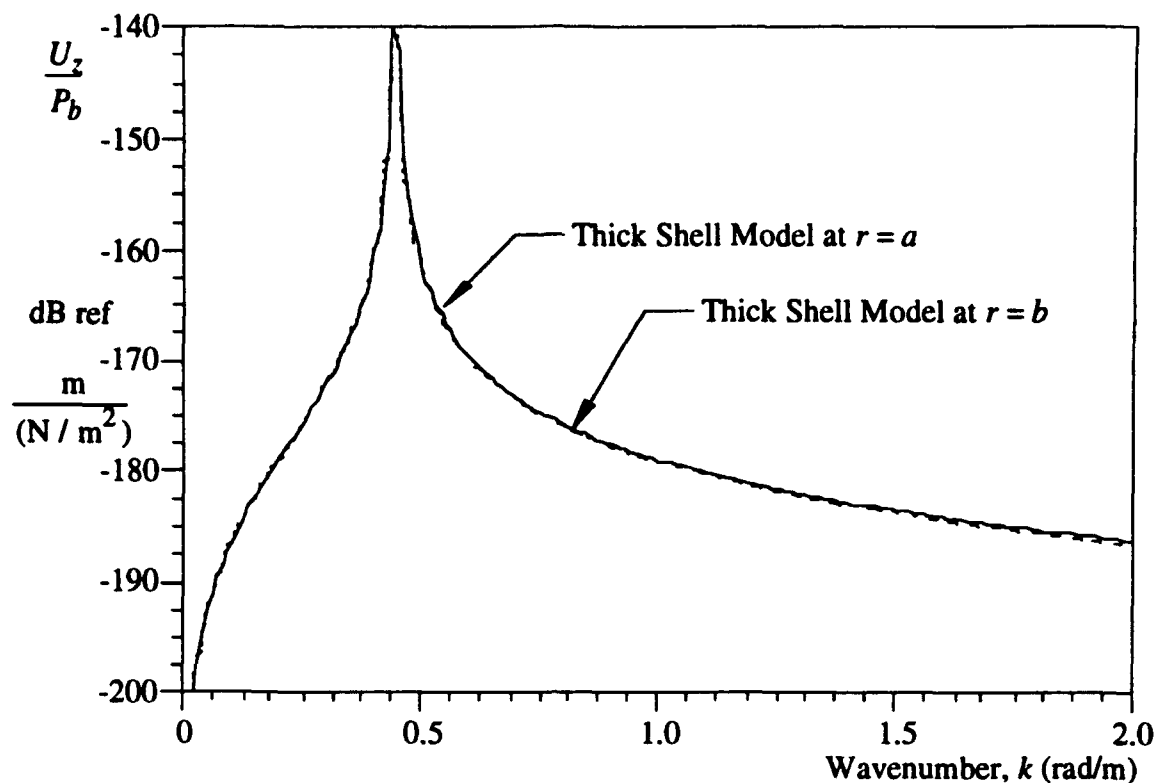


Figure 17. Magnitude of Axial Displacement Divided by Applied Radial Pressure: Comparison of Transfer Function at $r = a$ to $r = b$, $f = 50$ Hz, $2h/(a+b) = 1$

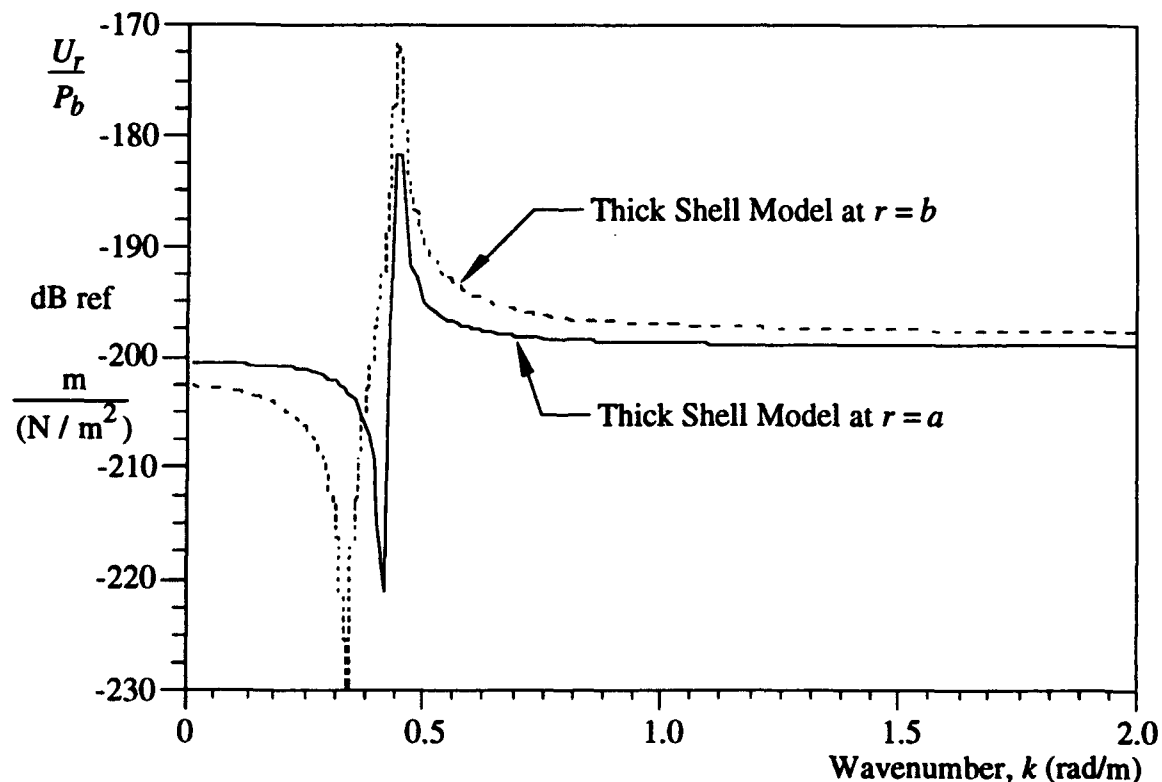


Figure 18. Magnitude of Radial Displacement Divided by Applied Radial Pressure: Comparison of Transfer Function at $r = a$ to $r = b$, $f = 50$ Hz, $2h/(a+b) = 1$

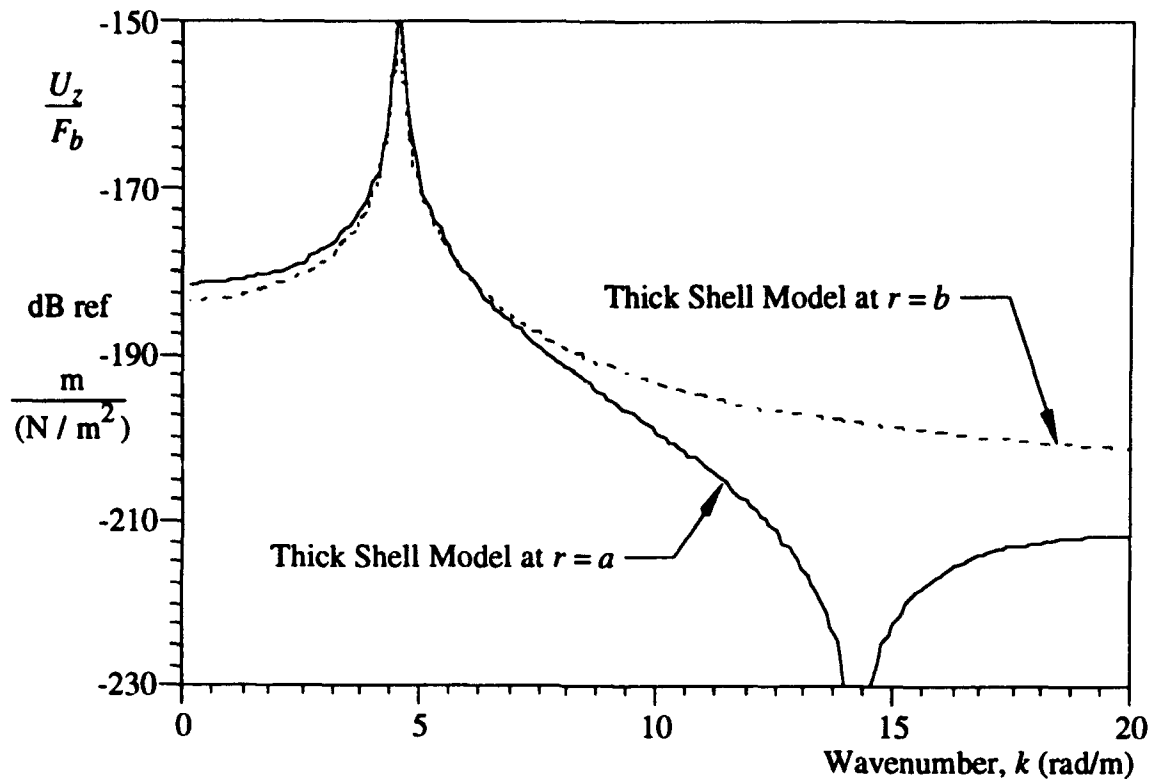


Figure 19. Magnitude of Axial Displacement Divided by Applied Axial Stress:
Comparison of Transfer Function at $r = a$ to $r = b$, $f = 500$ Hz, $2h/(a+b) = 1$

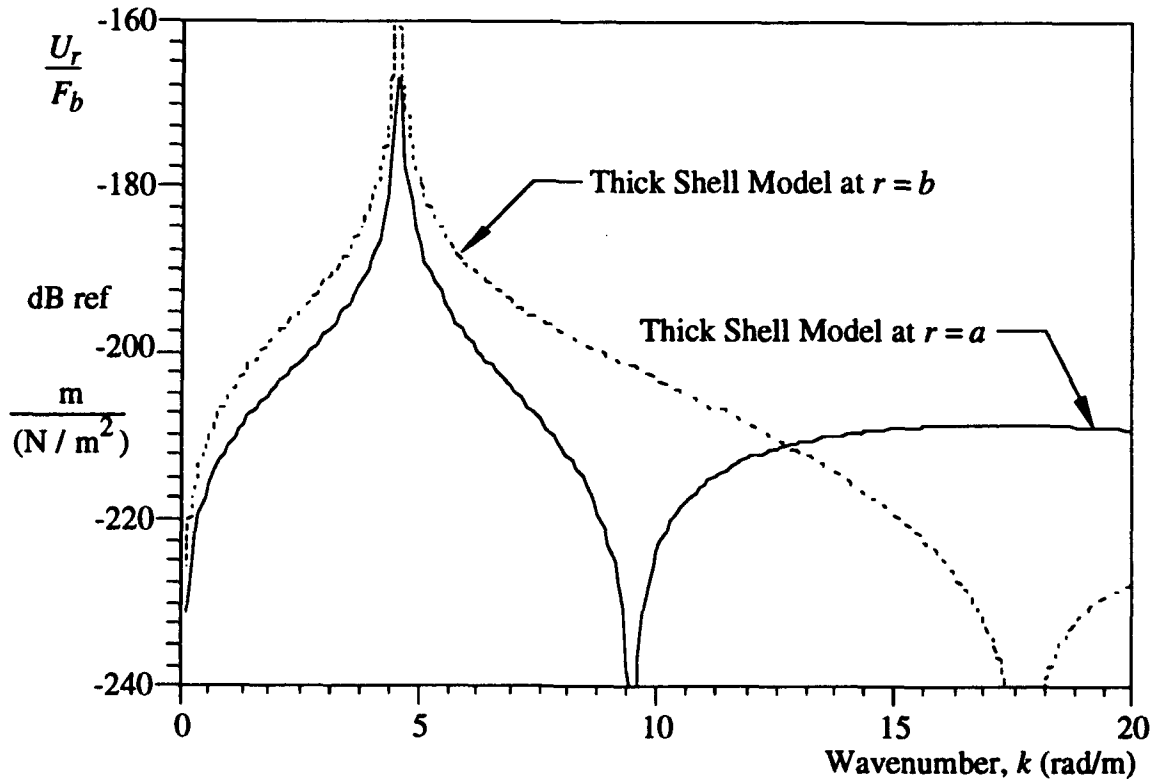


Figure 20. Magnitude of Radial Displacement Divided by Applied Axial Stress:
Comparison of Transfer Function at $r = a$ to $r = b$, $f = 500$ Hz, $2h/(a+b) = 1$

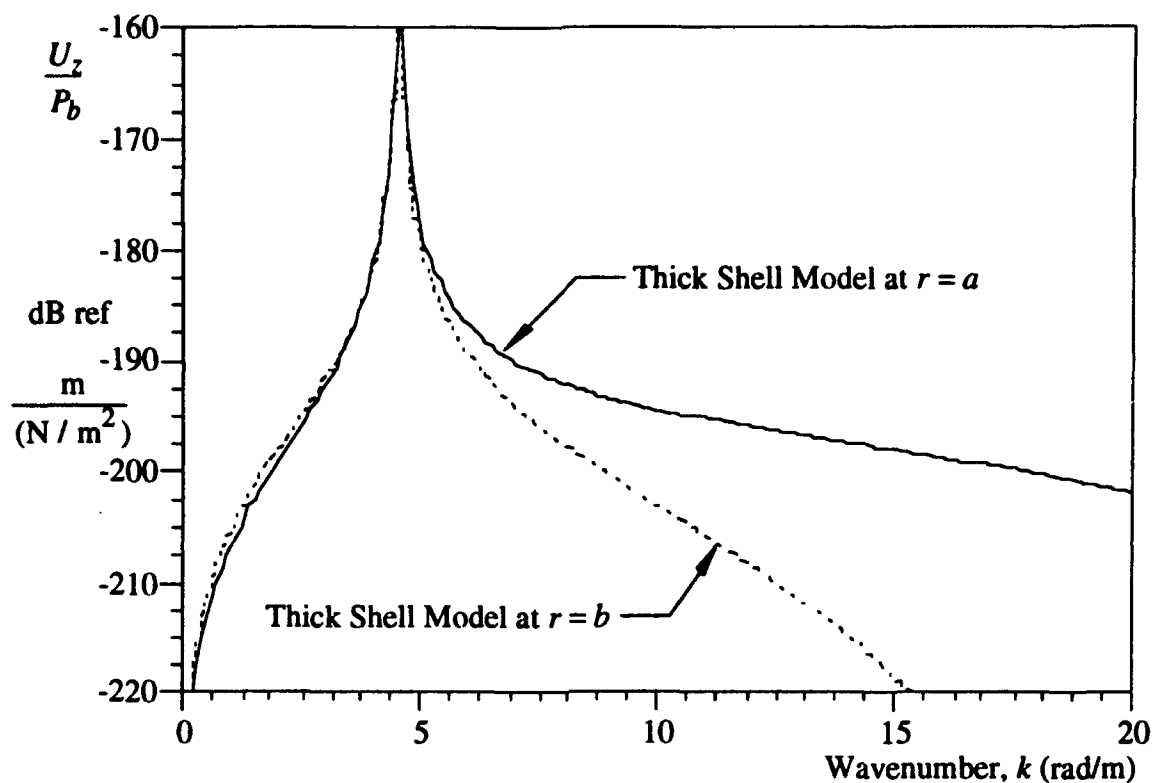


Figure 21. Magnitude of Axial Displacement Divided by Applied Radial Pressure: Comparison of Transfer Function at $r = a$ to $r = b$, $f = 500$ Hz, $2h/(a+b) = 1$

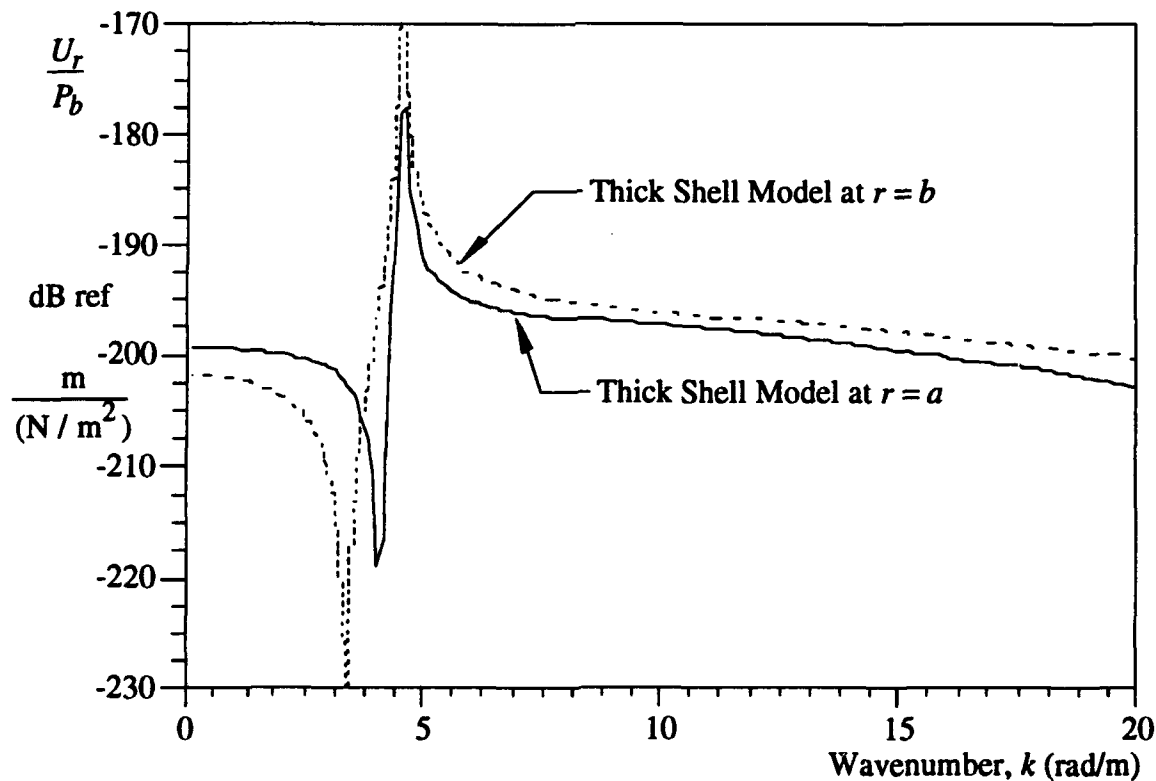


Figure 22. Magnitude of Radial Displacement Divided by Applied Radial Pressure: Comparison of Transfer Function at $r = a$ to $r = b$, $f = 500$ Hz, $2h/(a+b) = 1$

5. CONCLUSIONS

A model of an infinite length, axisymmetric, isotropic, forced thick shell response based on Bessel function solutions has been presented. This new model allows for displacement variations across the shell wall. The case of the mean radius of the shell equal to the shell thickness has been analyzed and compared to thin shell equations of motion. It is shown that, in general, the thin shell equations of motion tend to underpredict thick shell response.

6. REFERENCES

- Herrmann, G., and Mirsky, I., "Three-Dimensional and Shell-Theory Analysis of Axially Symmetric Motion of Cylinders," *Journal of Applied Mechanics*, pp. 563-568, 1956.
- Hull, A. J., "A Nonconforming Approximate Solution to a Specially Orthotropic Axisymmetric Thin Shell Subjected to a Harmonic Displacement Boundary Condition," *Journal of Sound and Vibration*, to appear 1994.
- McNiven, H. D., Shah, A. H., and Sackman, J. L., "Axially Symmetric Waves in Hollow, Elastic Rods: Part I," *Journal of the Acoustical Society of America*, Vol. 40, No. 4, pp. 784-792, 1966.
- Mirsky, I., "Axisymmetric Vibrations of Orthotropic Cylinders," *Journal of the Acoustical Society of America*, Vol. 36, No. 11, pp. 2106-2112, 1964a.
- Mirsky, I., "Vibrations of Orthotropic, Thick, Cylindrical Shells," *Journal of the Acoustical Society of America*, Vol. 36, No. 1, pp. 41-51, 1964b.
- Mirsky, I., and Herrmann, G., "Axially Symmetric Motions of Thick Cylindrical Shells," *Journal of Applied Mechanics*, pp. 97-102, 1958.
- Potter, M. C., *Mathematical Methods in the Physical Sciences*, Prentice-Hall, Inc., Englewoods Cliffs, New Jersey, 1978.

Timoshenko, S. P., and Goodier, J. N., *Theory of Elasticity*, McGraw-Hill Book Company,
New York, 1934.

APPENDIX - DERIVATIVES OF THE BESSEL FUNCTIONS

The following equations are derivatives of the Bessel functions used in section 2:

$$\frac{d}{dr}[J_0(\alpha r)] = -\alpha J_1(\alpha r) , \quad (\text{A-1})$$

$$\frac{d}{dr}[J_1(\alpha r)] = \frac{\alpha}{2}[J_0(\alpha r) - J_2(\alpha r)] , \quad (\text{A-2})$$

$$\frac{d}{dr}[J_2(\alpha r)] = \frac{\alpha}{2}[J_1(\alpha r) - J_3(\alpha r)] , \quad (\text{A-3})$$

$$\frac{d}{dr}[Y_0(\alpha r)] = -\alpha Y_1(\alpha r) , \quad (\text{A-4})$$

$$\frac{d}{dr}[Y_1(\alpha r)] = \frac{\alpha}{2}[Y_0(\alpha r) - Y_2(\alpha r)] , \quad (\text{A-5})$$

$$\frac{d}{dr}[Y_2(\alpha r)] = \frac{\alpha}{2}[Y_1(\alpha r) - Y_3(\alpha r)] , \quad (\text{A-6})$$

$$\frac{d}{dr}[K_0(\alpha r)] = -\alpha K_1(\alpha r) , \quad (\text{A-7})$$

$$\frac{d}{dr}[K_1(\alpha r)] = -\frac{\alpha}{2}[K_2(\alpha r) + K_0(\alpha r)] , \quad (\text{A-8})$$

$$\frac{d}{dr}[K_2(\alpha r)] = -\frac{\alpha}{2}[K_3(\alpha r) + K_1(\alpha r)] , \quad (\text{A-9})$$

$$\frac{d}{dr}[I_0(\alpha r)] = \alpha I_1(\alpha r) , \quad (\text{A-10})$$

$$\frac{d}{dr}[I_1(\alpha r)] = \frac{\alpha}{2}[I_2(\alpha r) + I_0(\alpha r)] , \quad (\text{A-11})$$

and

$$\frac{d}{dr}[I_2(\alpha r)] = \frac{\alpha}{2}[I_3(\alpha r) + I_1(\alpha r)] . \quad (\text{A-12})$$

INITIAL DISTRIBUTION LIST

Addressee	No. of Copies
Defense Technical Information Center	12
Naval Sea Systems Command (CAPT G. Kent (PMS-425), M. Basilica (PMS-4251), D. Lechner (PMS-42511))	3
Office of Naval Research, Code 321 (T. G. Goldsberry, K. Dial)	2
Program Executive Officer-Undersea Warfare, ASTO (CDR J. Polcari, W. Chen, A. Hommel, J. Jones, LCDR M. Traweck, R. Melusky)	6
Space and Naval Warfare Systems Command (J. P. Feuillet (PMW-182))	1
Michigan State University (C. R. MacCluer, C. J. Radcliffe)	2
Cambridge Acoustical Associates, Inc. (J. E. Cole, J. M. Garrelick)	2
Chase, Inc. (D. M. Chase)	1
Technology Service Corporation (L. W. Brooks)	1